Design and Synthesis of Nanostructured Peptoids Assemblies that Mimic Natural Carbonic Anhydrases

Haoyu Wang

A thesis

submitted in partial fulfillment of the

requirements for the degree of

Master of Science

University of Washington

2023

Reading Committee:

Chun-Long Chen

Elizabeth Nance

Program Authorized to Offer Degree:

Chemical Engineering

University of Washington

Abstract

Design and Synthesis of Nanostructured Peptoids Assemblies that Mimic Natural Carbonic Anhydrases

Haoyu Wang

Chair of the Supervisory Committee:
Chun-Long Chen
Chemical Engineering

Artificial Carbonic Anhydrase (CA) mimics that resemble natural CA have gained increasing attention recently due to their low-cost synthesis, high tunability, and high efficiency. However, it remains a significant challenge to precisely control nanostructure-based CA mimics and achieve high catalytic efficiency. Peptoids, poly-N-substituted glycines, offer unique advantages for this purpose because they can self-assemble into various nanostructures with high crystallinity and stability and serve as the template for precise control over the active sites that mimic CAs. By carefully designing the hydrophilic and hydrophobic regions of the peptoid and the terminal Zn-coordination site, the self-assembled peptoid materials showed excellent hydrolytic efficiency as CA mimics to hydrolyze p-nitrophenyl acetate (p-NPA), a model substrate for testing the esterase catalytic activity. Moreover, the peptoid CA mimics can be

operated under basic conditions yielding higher activity. The importance of nanostructure to catalytic efficiency was also demonstrated by comparing numerous control studies. Finally, some other peptoids, which self-assemble into helices, rods, and sheets, are presented to have the potential for developing CA mimics in the future.

TABLE OF CONTENTS

ACKNOWLEDGEMENTS

I would like to express my sincerest and deepest gratitude to my advisor, Dr. Chun-Long Chen, for his dedicated instruction, guidance, and support of my research. I would like to thank Dr. Shuai Zhang for his guidance and management in NanoES 280 Lab. Additionally, I gratefully appreciate Dr. Hoang for her valuable help on my p-NPA hydrolysis experiment, including designing the experiment, data analysis, and the LCMS spectra. Moreover, I appreciate Dr. Progyateg for his instruction on my hydrolysis experiment and thesis formatting. I would also appreciate all my lab mates, Renyu, who synthesized most of the peptoids for my research, Wenhao, who gave me the best AFM instruction, Emily, who helped me with operating UV-vis and a variety of chemical materials, and Reagan, Zhihao, Minyang, Francis, Qizheng, who helped with my experiments. I am thankful for Prof. Nance to be my committee member. I would like to express my appreciation to the CSSAS for providing the interdisciplinary platform to inspire my thinking and cutting-edge research tools. Finally, I would like to thank my family and friend for their constant support and encouragement on my academic journey.

DEDICATION

To Dr. Chun-Long Chen, my esteemed advisor and mentor, whose guidance and support have been indispensable to my academic road.

Chapter 1. INTRODUCTION

1.1 CA AND CA MIMICS

Increasing carbon dioxide (CO_2) in the atmosphere causes the greenhouse effect, which leads to global warming [1]. It has been reported that 37.12 billion tons of CO_2 were emitted into the atmosphere in 2021, and the emission growth is still not reaching its peak [2]. Slowing down the greenhouse effect is a crucial task for sustainable human society development. Carbonic anhydrase (CA) is a zinc-containing metalloenzyme, one type of hydrolase that participates in many important physiological processes [3]. CA can catalyze CO_2 hydration into bicarbonate ions (HCO_3^-), sequestering CO_2 from the atmosphere to reduce the global warming effect. So far, there are eight CA species (families) discovered, categorized by Greek alphabet (α, β, γ, δ, ζ, η, θ, ι) [4]. Among them, human CA II from α family is well-studied on an atomic scale and suitable for mechanistic study [5].

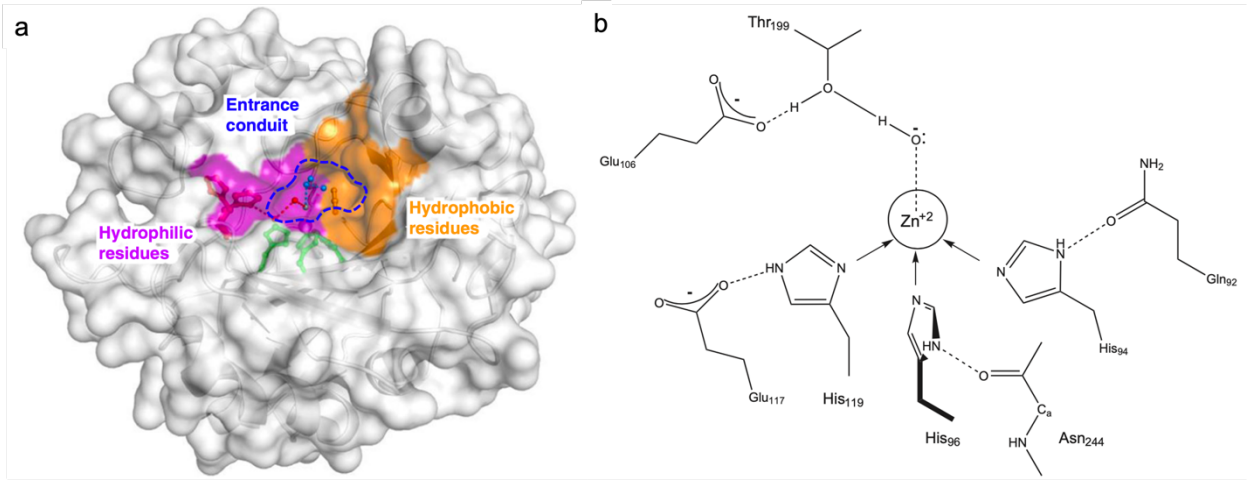

Figure 1-1. (a) The CA protein model shows the cone-shaped cavity where the Zn active site is located, and the region is divided into three parts with different functions: the hydrophobic/hydrophilic parts and the entrance conduit (EC). Reproduced from Kim et al. [5]. (b) The molecular coordination details of the active site of human CA II. Reproduced with permission from reference [6].

CA II has an active site Zn^{2+} located at the bottom of a 15 A˚ depth cone-shaped cavity, and this region is divided into three parts with different functions: (1) the hydrophobic residues can bind with the substrate (ex. CO_2); (2) the hydrophilic residues are responsible for water, product, and substrate exchange; and (3) an entrance conduit connects the hydrophobic and hydrophilic parts [6,7]. The Zn^{2+} is coordinated to three nitrogen atoms on the imidazole group from His-94, His-96, and His-119, and an oxygen atom from either one H_2O or OH^- to form a tetrahedral geometry [8,9]. The CO_2 hydration mechanism by CA is illustrated in Figure 1-2. At the zinc center, the pKa of the Zn-bounded water is 7, which allows the water molecule to be relatively easily deprotonated under a physiological environment compared to the bulk water [5]. After Zn-bounded water is deprotonated, the resulting hydroxyl group can perform a nucleophilic attack at a CO_2 molecule. Subsequently, a Zn-bounded bicarbonate ion (HCO_3^-) as an intermediate molecule is formed. The HCO_3^- on the Zn active site is then substituted by a free H_2O. The H_2O on the Zn^{2+} is deprotonated to recover the initial Zn-hydroxyl form [5,9]. In the hydration reaction, the deprotonation of the bound water is considered the rate-limiting step for the whole reaction [10].

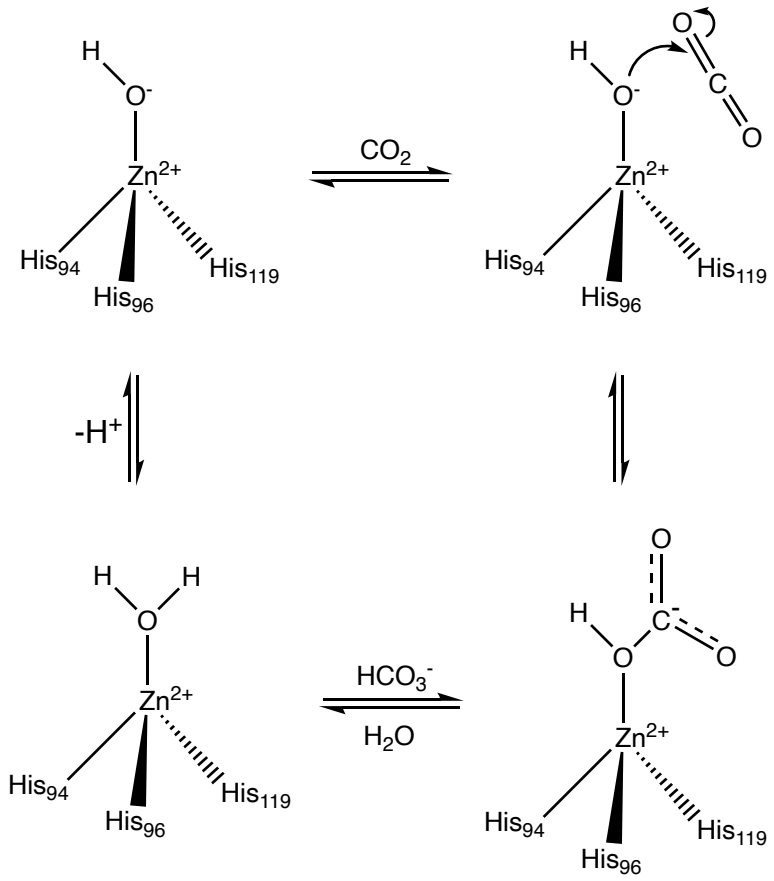

Figure 1-2. The CO_2 hydration mechanism by CA II [6,8,9,11].

Artificial CA mimics have gained increasing attention recently due to a series of advantages over natural CA enzymes [7,9,12]. CA mimics have a similar active site and catalytic mechanism resembling natural CA. However, unlike natural CAs, CA mimics are easy to be synthesized with lower cost and higher tunability. They have a higher thermostability, when operating hydration reactions under higher temperatures, and can also resist many different reaction environments other than physiological environments. These advantages make CA mimics an ideal model for developing CO_2 sequestration technologies [7,9,12]. There are several types of CA mimics, including cyclic small-molecule CA mimics, like zinc-cyclen, zinc-tri, and zinc-cyclam, which were synthesized and studied (Figure 1-3 a-c) [11,13]. These molecules can trap Zn^{2+} in the molecular cycle by coordinating with nitrogen atoms in the cyclic molecules. Tris(2-

benzimidazolylmethyl)amine ligand (L1) and its derivatives Figure 1-3 (d), which have three nitrogen donors from three imidazole groups and hydrophobic pockets, are also used for constructing highly efficient small-molecule CA mimics [10,14].

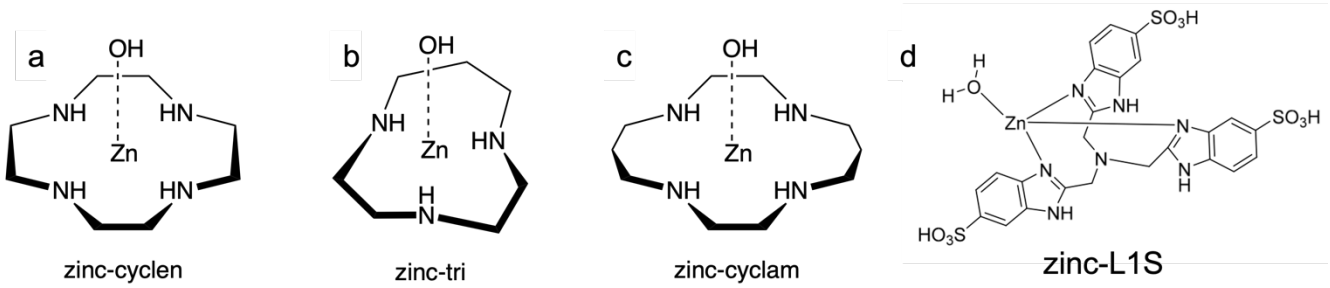

Figure 1-3. Several small molecule CA mimics. (a) zinc-cyclen; (b) zinc-tri; (c) zinc-cyclam; (d) zinc-L1S. Reproduced from Ma et al. [11] and Rains et al. [10]. Copyright © 2019, American Chemical Society.

Instead of designing small molecule CA mimics, the metal-organic framework (MOF) is also a good platform to construct CA mimics. Wright et al. used MOF MFU-4l ($Zn_5Cl_4(BTDD)_3$, where BTDD = bis(1,2,3-triazolo[4,5-b],[4',5'-i])dibenzo[1,4]dioxin) to build CA mimics [15]. MFU-4l has secondary building units (SBUs) that are very similar to the CA active site, and the activity of the catalytic site was improved by exchanging the Cl- anion with OH- from organic hydroxide. Jin et al. also demonstrated that MOF could mimic CA and convert CO_2 into HCO_3^- [16]. They used CFA-1, which has a central Zn coordinated with six triazole nitrogen atoms and four other Zn coordinated with three triazole nitrogen atoms. These Zn-nitrogen complexes have a similar active site to CA and showed nice performance in both absorptions of CO_2 and conversion of CO_2 into HCO_3^-. However, these CA mimics only imitated the active site of CAs, and did not have the local environment which could promote the water, product, and substrate exchange as the natural CA does.

To address those challenges, recently synthetic peptides, peptide assemblies, and designed proteins have also been exploited to develop highly efficient CA mimics [17–19]. Also, using peptides to mimic CA can achieve a high similarity and environment-friendly catalysis. Six peptides with seven or eleven residues that can form an amyloid-like structure were designed and synthesized by Al-Garawi et al. [12]. These peptides have an alternating pattern of hydrophobic isoleucine (I) and hydrophilic histidine (H) amino acids, while the sixth amino acid is substituted as tyrosine (Y) for amyloid structure formation. They can self-assemble into β-sheet and bind with Zn^{2+} to form an activation site, which mimics CA, catalyzing the hydrolysis reaction of p-NPA, which is a chromogenic compound used for assessing hydrolytic enzymes' activity. In contrast, the peptides assembled in the absence of Zn^{2+} showed no catalytic activity. This research demonstrates that the self-assembled materials that can form correct and suitable metal binding microstructure are essential to creating an effective catalytic site further.

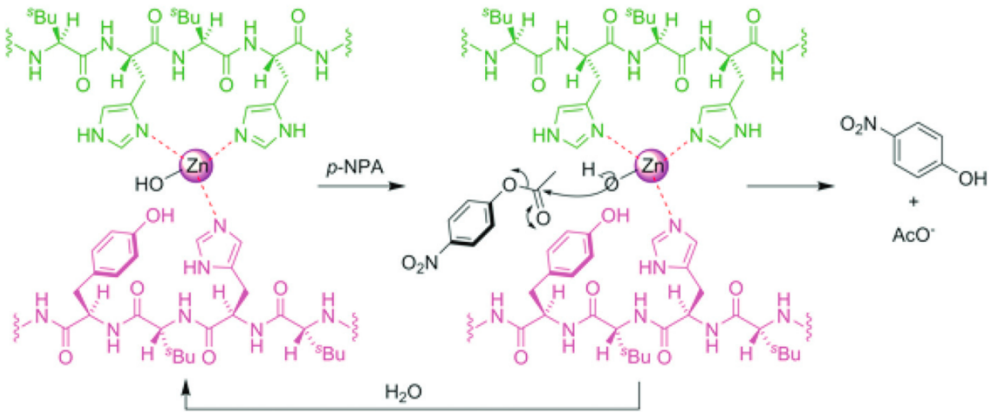

Figure 1-4. The mechanism of hydrolysis of p-NPA by self-assembled fibrils of amyloidogenic peptide (Ac-IHIHIYI-NH_2) . The self-assembled peptide contains a catalytic Zn-binding site that forms a $Zn(His)_3$–OH quaternary coordination geometry. Reproduced with permission from Al-Garawi et al. [12]. Copyright 2017 Royal Society of Chemistry.

While peptide-based materials offer great potential in developing highly efficient CA mimics and demonstrate that the morphologies of peptide assemblies and the local environment of catalytic

sites are significant for the CA-like catalytic activities, it remains a significant challenge in precisely controlling over the morphologies and local environment of peptide assemblies. Predicting the structure and assembly of peptides and their functions can be challenging after even a single amino acid residue is modulated. Furthermore, similar to natural enzymes, peptide-based materials often suffer from their poor stabilities after exposure to elevated temperature or proteolytic degradation.

1.2 Peptoids and Peptoid Synthesis

Nanostructures are materials that have at least one dimension with a length scale of 1–100 nm length scale [20]. Recently reported organic nanostructures include one-dimensional (1D) organic nanotubes [21,22], two-dimensional (2D) organic membrane-mimetic nanosheets [23–25], and nanohelices hierarchical nanosheets [26,27]. These nanostructures can provide a platform to develop biomimetic materials for application in a variety of fields, like biomineralization, bioimaging, bio-catalysis, pharmaceutics, etc. [28–31].

Peptoids, poly-N-substituted glycines, are sequence-defined synthetic organic molecules developed to bridge the advantages of bulk polymers and biopolymers. Compared to peptides, the side-chain position of peptoids is shifted from α-carbon by one atom to the nitrogen in an amide unit (Figure 1-5) [32]. As a result of changing the side-chain position, peptoids lack hydrogen bond donors from the amide group, making the peptoid inter- and intra- molecular forces simpler. The cancellation of hydrogen bonding will also let the peptoids' properties be dominated by the side-chain and monomer chemistry [33]. Thus peptoids are more chemically and thermally stable than peptides and proteins and have more flexibility to tune their functions [22,24,34]. Moreover, we

can manipulate both peptoid-peptoid and peptoid-substrate interactions to engineer peptoid-based nanostructures [35]. For example, two-dimensional crystalline peptoid sheets were engineered by manipulating the peptoid-peptoid interactions [23].

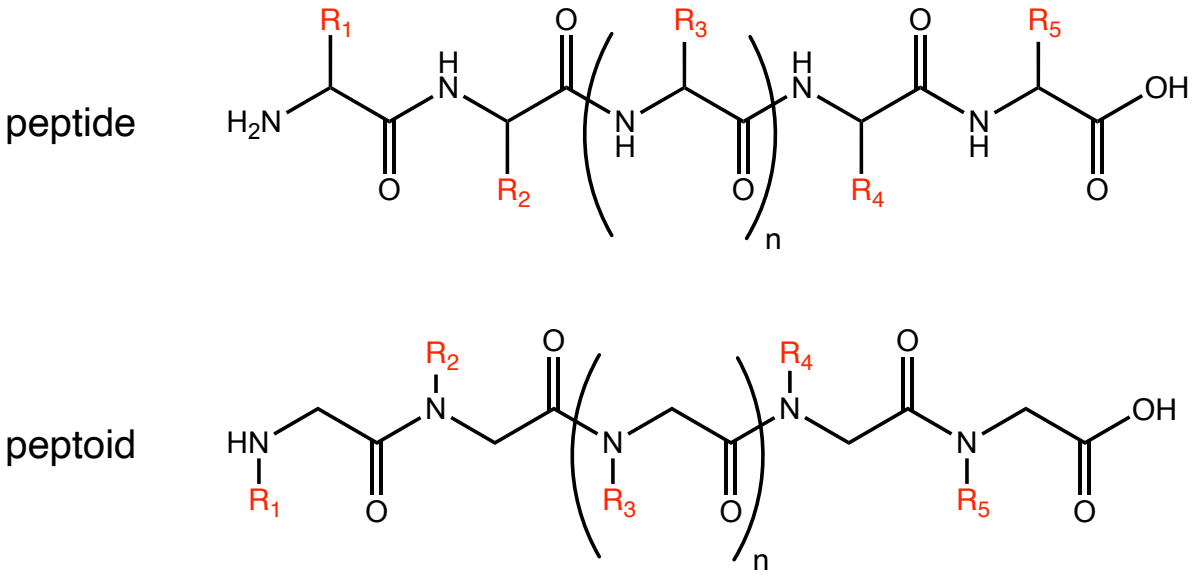

Figure 1-5. Peptides vs peptoids. Compared to peptides, the side-chain of peptoids is shifted from α-carbon to nitrogen and the hydrogen bond donor is canceled on the nitrogen.

Peptoids can be synthesized by the solid-phase synthesis method [32,33,36]. The reaction starts from a resin-bound amine; then in the first step, an acylation occurs in which a haloacetic acid (usually bromoacetic acid) reacts with the amine to form amide. In the second step, a primary amine with desired side chain displaces the halogen (ex., bromine) by a nucleophilic S_N2 displacement in the amide formed in the first step. Since the displacement reaction is an S_N2 progress, the side chain of the amines with nucleophilic centers should be protected to avoid undesired reactions. The acylation and S_N2 displacement steps are repeated alternatively until the targeted peptoid is synthesized. This acylation and displacement cycle can allow the peptoid reaches a polymerization degree of up to 50, and each cycle can reach a yield of 99% [36]. Then the final peptoid crude product is cleaved from the resin, as well as the side chain is de-protected

under the effect of 95% trifluoroacetic acid (TFA). The peptoid synthesis protocol is shown in Figure 1-6. Using the solid-phase synthesis method, we can achieve precise control over the peptoid sequence with exact monomer placement, leading to finer control of the peptoid chemical properties [33]. Also, since there are hundreds of amines commercially available in gram quantities, a wide variety of peptoids can be designed and synthesized from tremendous combinations of these amines [32].

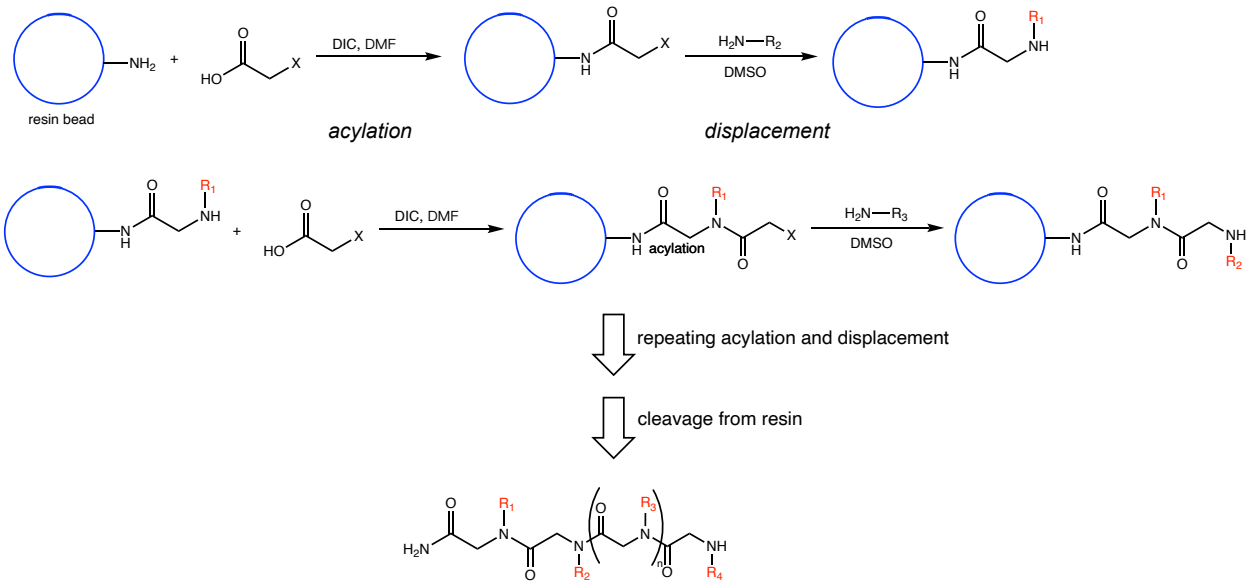

Figure 1-6. Sequence-specific peptoids synthesis by a repeating two-step cycle of acylation and displacement. After reaching the desired peptoid sequence, 95 % TFA is applied to cleave the peptoid from the resin bead.

1.3 Using Peptoid to Build Enzyme Mimetics

Peptoids can be a platform to mimic how nature produces the diversity of biopolymers and understand the interactions between organic and inorganic molecules. Recently, our group has utilized peptoid-peptoid interactions to build various peptoid nanostructures, and their properties like structural parameters, stability, and assembling mechanism are studied in detail (Figure 1-7) [22,24].

These peptoids are easy to synthesize and can self-assemble into nanostructures. The surface chemistry of peptoid self-assemblies can be tuned precisely by modifying the peptoid sequence chemistry. And the self-assembled structures have excellent stabilities under basic, elevated temperatures and pure organic solvent conditions. They often exhibit strong mechanical properties as a result of high crystallinity, which offers great potential for micromechanical applications and nanodevices. Peptoid nanostructures have already shown their potential for controlling quantum dots (QDs) arrangement by modifying peptoid end groups based on the tube and sheets forming peptoid [37,38].

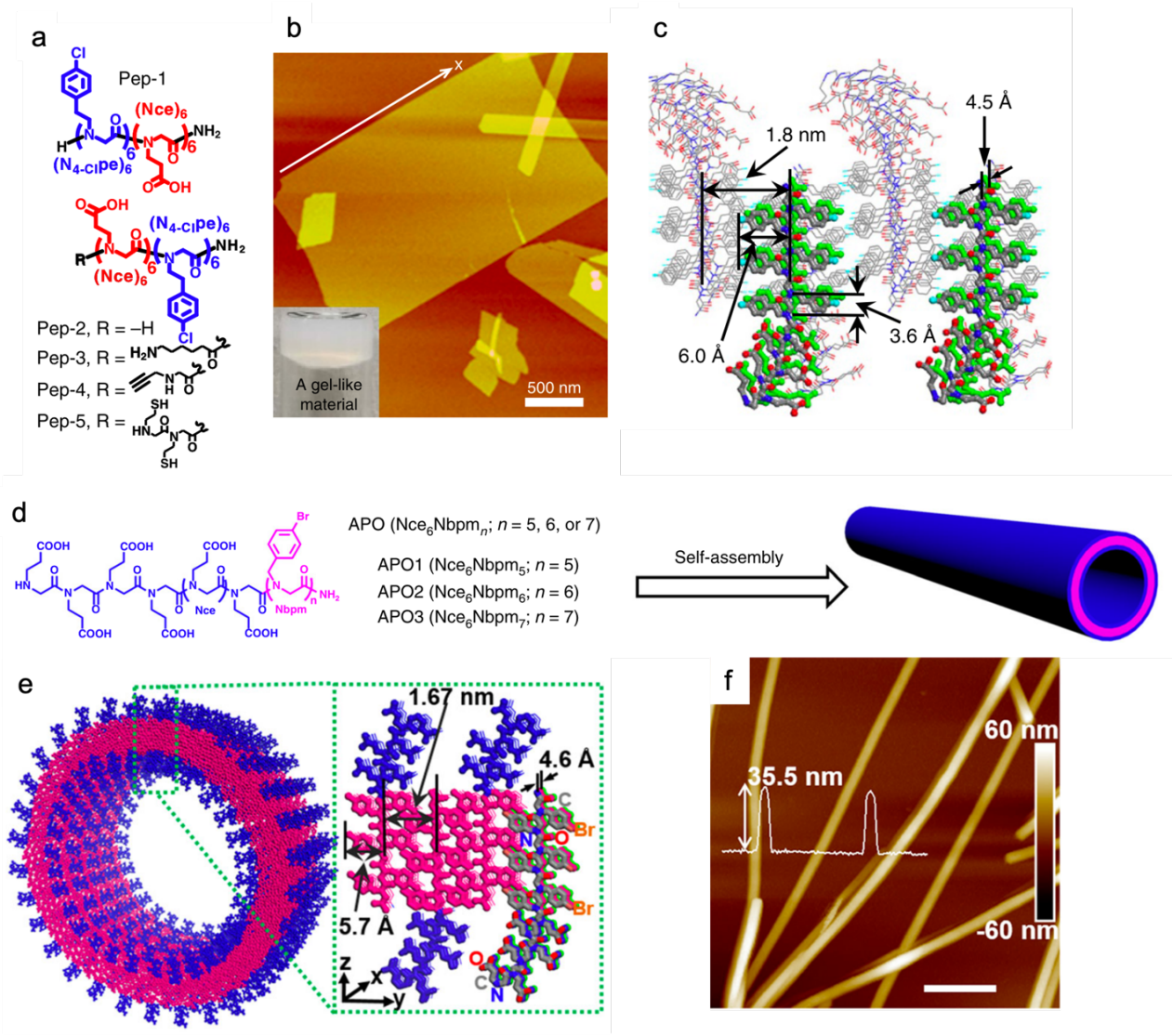

Figure 1-7. (a) The molecular structures of the sheets forming peptoids. (b) AFM images of self-assembled peptoid nanosheets (Nce_6Ncpe_6). (c) The molecular packing model of ($Ncpe_6Nce_6$) membrane, in which the peptoid backbone-to-backbone distance is 4.5 Å along the x direction and is 1.8 nm along the y direction. (d) The molecular structures of the tube-forming peptoids, in which the peptoid backbone-to-backbone distance is 4.6 Å along the x direction and is 1.67 nm along the y direction. The blue part indicates the hydrophilic domain, while the pink part indicates the hydrophobic domain. (e) The molecular packing model of (Nce_6Nbpm_6) tubes. (f) AFM images of self-assembled peptoid nanosheets (Nce_6Nbpm_6). Reproduced from Jin et al. [22,24].

These peptoid structures also showed more robust stability compared to peptides and proteins with similar units, allowing us to use them as templates and incorporate functional groups to build

functional nanomaterials. For example, Jian et al. developed a series of self-assembled peptoid/hemin nanotubes to mimic natural peroxidases that can depolymerize lignin [39]. They found that peptoid nanotubes containing Npyr, which can strongly bind hemin, have the best catalytic activity toward a model compound ABTS. Also, the peptoid/hemin complexes showed excellent catalytic efficiency toward lignin degradation. As the authors proposed, the multiple highly ordered catalytic site on the nanotube can simultaneously react with lignin, while the peroxidase containing a single active site cannot cleave the bonds in lignin. This research showed the great prospect of using peptoid self-assembly nanostructure to build other enzyme mimics and even achieve some functionalities its natural counterpart does not possess. As part of our ongoing efforts to develop peptoid mimics, we are exploring different conjugation strategies, including covalent attachment of functional groups to peptoid structures.

Similarly, as the research mentioned above, by combining the unique properties of self-assembled peptoids materials like high crystallinity and easy-to-tune surface chemistry, self-assembled peptoids nanomaterials offers great potential for the design and synthesis of nanostructured CA mimics for promoting CO_2 hydration. By doing so, we can combine the advantage of the strong catalyzing activity of ligands and the hierarchy and stableness of peptoid self-assemblies in one platform. However, despite the tremendous side-chain diversity of peptoids, predictive synthesis of peptoids with desired catalytic activity remains a challenge. This research will exhibit and discuss the recent advances in using peptoid self-assemblies to build CA mimics and assess their catalytic ability by performing p-NPA hydrolysis experiments.

Chapter 2. MATERIALS AND METHODS

2.1 MATERIALS

Bromoacetic acid and succinic anhydride (Suc) were purchased from Chem-Impex International, Inc. Rink amide AM resin was purchased from Supra Sciences. N,N'-diisopropylcarbodiimide (DIC), 4-methylpiperidine (PIP), trifluoroactic acid (TFA), 4-bromophenethylamine (NBrpe), 4-bromobenzylamine (NBrpm), tert-butyl N-(2-aminoethyl)carbamate (Nae), β-alanine tert-butyl ester hydrochloride (Nce) were purchased from Oakwood Chemical. Diglycolic anhydride (Dig) was purchased from TCI Chemicals. Fmoc-Gly-OH (Nc2), Fmoc-b-Ala-OH (Nc3) were purchased from Aapptec. 4-nitrophenol (p-NP), 4-nitrophenyl acetate (p-NPA), dichloromethane (DCM), dimethylformamide (DMF), 4-(2-hydroxyethyl)-1-piperazineethanesulfonic acid (HEPES), LC/MS graded acetonitrile (ACN), zinc tetrafluoroborate hydrate ($Zn(BF_4)_2 \cdot xH2O$), and N-methyl-2-pyrrolidone (NMP) were purchased from Fisher Scientific. DO3A-tert-butyl ester was purchased from AmBeed. HPLC graded water was purchased from Sigma-Aldrich. MilliQ water at 18 MΩ cm was used for all experiments.

2.2 PEPTOID SYNTHESIS

For manual solid-phase synthesis, rink amide resin (0.09 mmol) was used to synthesize C-terminal amphiphilic peptoids. In the synthesis procedure, the Fmoc groups on the resin were deprotected by adding 2 mL of 20% (v/v) PIP/DMF, agitating for 40 min, filtering, and washing with DMF. For all DMF washes, 1 mL DMF was added and then agitated for 1 min (repeated five times). An acylation reaction was then performed on the amino resin by the addition of 1.5 mL of 0.6 M

bromoacetic acid in DMF, followed by adding 0.30 mL of 50% (v/v) DIC/DMF. The mixture was agitated for 10 min at room temperature, filtered, and washed with DMF for five times. Nucleophilic displacement of the bromine with different primary amines occurred by the addition of 1.5 mL of 0.6 M primary amine monomer in NMP, followed by agitation for 10 min at room temperature. The monomer solution was filtered from the resin and washed with DMF for five times. The acylation and displacement steps were repeated until the targeted amphiphilic peptoid was synthesized.

The final crude product was cleaved from the resin by adding 95% trifluoroacetic acid (TFA) in water, which was then evaporated under vacuum with Biotage V-10 evaporation system. Finally, crude peptoids were dissolved in H_2O/CH_3CN (v/v = 1:1) for HPLC purification. The crude products were purified by reverse-phase HPLC on a XBridge Prep C18 10 μm OBDTM (10 μm, 19mm × 100 mm), using an adaptable acetonitrile gradient in H_2O with 0.1% TFA over 15 min. Purified peptoids were analyzed using Waters ACQUITY reverse phase UPLC (corresponding gradient at 0.4 mL/min over 7 min at 40 °C with a ACQUITYBEH C18, 1.7 μm, 2.1 mm× 50mm column) that was connected with a Waters SQD2 mass spectrometry system. The final peptoid product was lyophilized twice from its water and acetonitrile (v/v = 1:1) solution. The peptoid powder was finally divided into small portions (1.0 × 10−6 mol) and stored at room temperature.

To synthesize Dig-containing sequences, 200 mg of Diglycolic anhydride, 0.016 g DMAP, 1 mL pyridine, and 2.5 mL DCM were added to Npm4 resin. The mixture was agitated at room temperature overnight, filtered, and washed with DCM 5 times.

To synthesize NBrpe6DO3A and NBrpe6Nce6DO3A, 1.5 mL of 0.6 M bromoacetic acid in DMF, and 0.30 mL of 50% (v/v) DIC/DMF was added to the peptoid resin first. The mixture was agitated for 10 min at room temperature, filtered, and washed with DMF five times. Then 200 mg of DO3A-tert-butyl ester, 24.8 mg of K_2CO_3, and 3 mL DMF was added to the resin. The mixture was mixing at room temperature for shaking overnight and washed with DMF and DCM five times. For the cleavage of DO3A peptoids, the peptoid resin need to mix with 95% TFA for five hours to remove the tert-butyl groups.

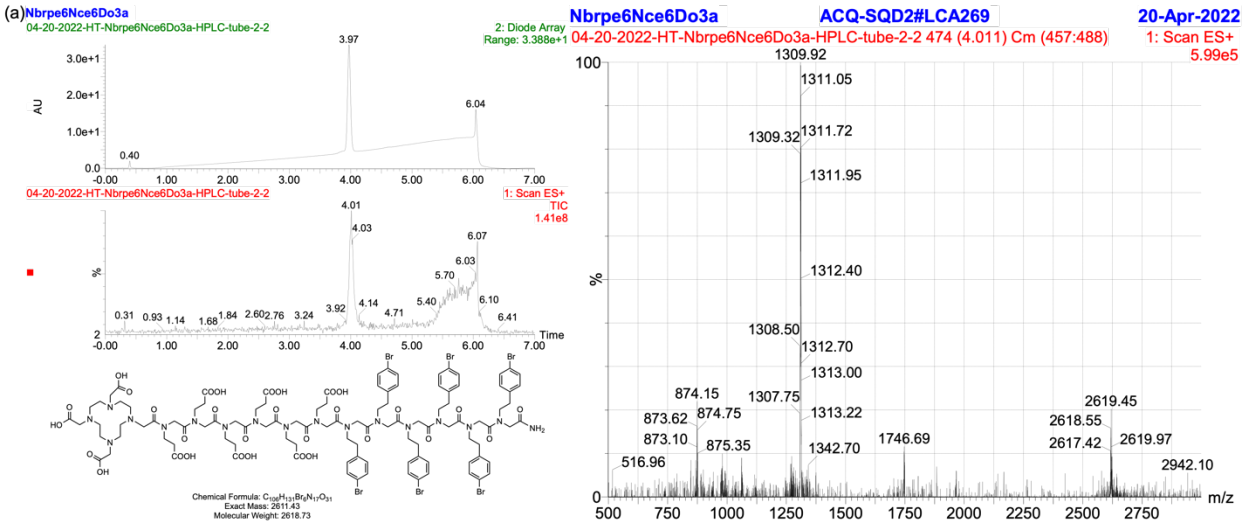

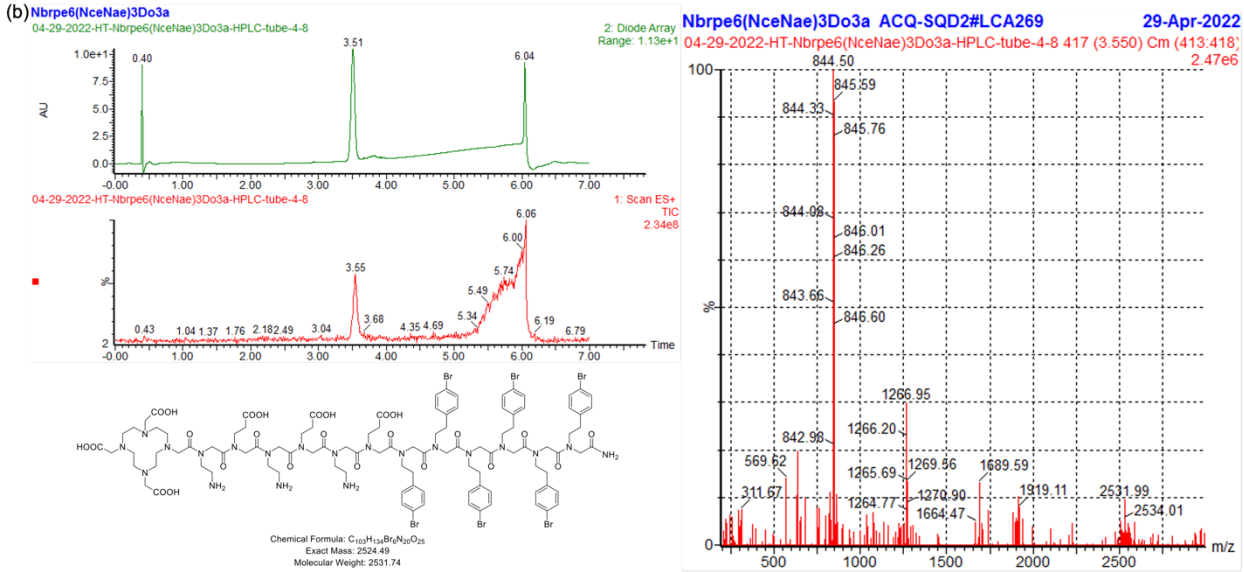

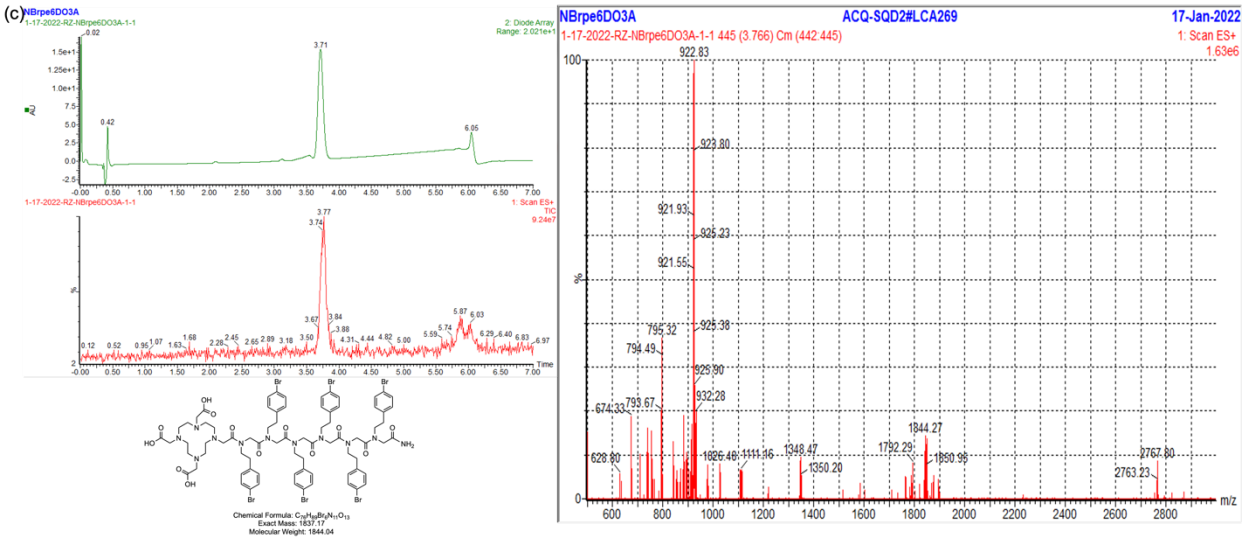

Figure 2-1. Representative LC-MS data and the corresponding peptoid structure: (a) NBrpe$_6$Nce$_6$DO3A, (b) NBrpe$_6$(NceNae)$_3$DO3A, and (c) NBrpe$_6$DO3A

2.3 PEPTOID SELF-ASSEMBLY

Npm series (Npm$_4$Dig, Npm$_5$Dig, Npm$_6$Dig, Npm$_4$, Npm$_4$Nc$_2$, Npm$_4$Nc$_3$) peptoids: 1 umol peptoid powders were dissolved in 200 uL water and acetonitrile (v/v = 1:1) solution to form a 5.0 mM peptoid solution, pH ranging from 4 ~ 6 measured by pH paper. The peptoid solution was stored in a 4 ℃ refrigerator for slow evaporation. After three days of evaporation, gel-like materials or white precipitates in clear solution were observed. The evaporation time could be varied according to the solution state. Then the cap of the vial was closed tightly to prevent further evaporation.

NBrpe series (NBrpe$_6$DO3A, NBrpe$_6$Nce$_6$DO3A, NBrpe$_6$(NceNae)$_3$DO3A) peptoids: 1 umol peptoid powder was dissolved by a small amount of 95% trifluoroacetic acid (TFA), then clear red solution is observed. Then the peptoid TFA solution was dried by N_2 gas flow, and the remnants were dissolved in water and acetonitrile (v/v = 1:1) solution to form a 5.0 mM peptoid solution, pH ranging from 1 ~ 3 measured by pH paper. Then the pH of the solution was tuned to 5 by a few drops of aqueous 1 M NaOH. The peptoid solution was stored in a 4 ℃ refrigerator for slow

evaporation. After three days of evaporation, white precipitates in a clear solution were observed. The evaporation time could be varied according to the solution state. Then the cap of the vial was closed tightly to prevent further evaporation.

For the DO3A group on the peptoid to be successfully conjugated with Zn ion, several self-assembling methods were explored. Here is a successful strategy for binding peptoid-DO3A with Zn ion: 0.5 umol pep-DO3A was dissolved in 200 uL acetonitrile, then 60 mM $Zn(BF_4)_2$ acetonitrile solution was added to the solution. The mixture was turbid at the beginning and turned clear after incubating with $Zn(BF_4)_2$ under R.T. overnight. The solution was lyophilized to get powder ① (peptoid-Zn and Zn salt). The powder ① was dissolved in 200 uL water and acetonitrile (v/v = 1:1), and the pH was checked. If the pH is not in the range of 5~6, the pH needs to be adjusted to 5~6. The peptoid solution was mixed thoroughly and stored in a 4 °C refrigerator for slow evaporation. After 14 days, the peptoid solution was refilled with water to 200 uL marker and continuously evaporated for days. After seven days, another 100 uL of water was added to the solution. White or light-yellow precipitates in a clear solution are observed during the process.

2.4 Transmission Electron Microscopy

TEM was conducted on the FEI Tecnai G2 F20 Supertwin TEM, operating at an accelerating voltage of 200 keV. The peptoid sample was characterized under both bright field mode and STEM mode. For TEM sample preparation, 1 uL peptoid self-assembly solution was diluted in 10 uL deionized water, and the mixture was transferred onto a pure carbon 300 mesh copper grid for 10 minutes. The liquid was blotted with filter paper. For the negative staining, 5 uL phosphotungstic

acid (PTA) (wt 2%) was added onto the grid for 2 minutes immediately after blotting the sample liquid. Finally, the PTA liquid was blotted with filter paper.

2.5 Atomic Force Microscopy

Ex situ (in air) AFM experiments were performed on a Bruker Icon using tapping mode or Peakforce mode under room temperature. For AFM sample preparation, typically, 1 uL assembly solution was diluted with 40 uL deionized water and dropped onto a freshly peeled mica substrate for 10 minutes. The liquid was blotted by Kimwipe and then dried by N_2 gas flow.

2.6 Peptoid CA Mimics Activity Test

The peptoid CA mimics hydrolytic activities were determined by the hydrolytic reaction of 4-nitrophenyl acetate (p-NPA) under room temperature [9,40–42]. P-NPA hydrolyzed by peptoids can produce p-nitrophenol (p-NP), which has the highest absorbance at the wavelength of 402 nm (Figure 2-2). P-NPA is commonly used as a model substrate for testing the esterase catalytic activities because the mechanism of p-NPA hydrolysis by CA and CA mimics is similar to the mechanism of CO_2 hydration by CA and CA mimics [43].

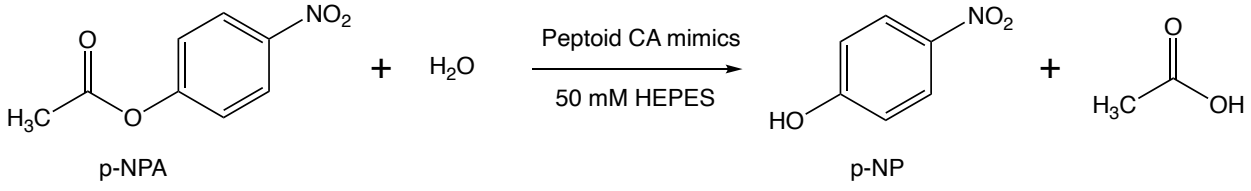

Figure 2-2. p-NPA hydrolysis reaction by peptoid CA mimics

In the hydrolysis experiment, 40 mM p-NPA in acetonitrile solution was prepared in advance. An 80 uL 0.167 mM aqueous solution of self-assembled peptoid materials was prepared in a 4 mL

vial with a stir bar. Then 880 uL 50 mM HEPES buffer (pH = 7.4) was added to the vial and placed on a stirring plate to start mixing. The concentrations of the reaction system are [peptoid] = 13.9 uM and [HEPES] = 45.8 mM.

The UV-vis measurements were conducted on NanoDrop oneC by the nanodrop functions. The automated pathlength was enabled to prevent absorbance oversaturation. 45.8 mM HEPES (water/50 mM HEPES = 1:11) was used as a blank for the system, and the premixed peptoid buffer solution was measured three times to record its blank. Then 4 uL 40 mM p-NPA ACN solution was added to the vial to trigger the reaction, and the solution was mixed immediately to take the first three measurements at 402 nm. Then, every 30 minutes, the UV-vis measurement was taken three times and continuously measured for 4 hours. The control experiments were conducted by replacing the 80 uL peptoid solution with pure water or 1 mM $Zn(BF_4)_2$.

For calculating the conversion of p-NPA, a standard curve of the product p-NP in a series of concentrations (0-200 uM) corresponding to the UV-vis absorbance at 402 nm was plotted. The experiment for preparing the standard curve is: preparing 40 mM p-NP in acetonitrile solution and 45.8 mM HEPES buffer (water/50 mM HEPES = 1:11) first. Then 200 uM p-NP solution was prepared by diluting 40 mM p-NP with 45.8 mM HEPES buffer, followed by mixing the 200 uM p-NP solution with 45.8 mM HEPES buffer in a different ratio, forming a series concentration of p-NP solution with similar solution condition to the p-NPA hydrolysis (Table 2-1). The UV-vis measurements were taken three times at 402 nm for each p-NP solution.

Table 2-1. The preparation for serial concentration p-NP solutions

p-NP concentration (uM)	p-NP solution added (uL)	45.8 uM HEPES buffer added (uL)
0	0	200
40	40	160
80	80	120
120	120	80
160	160	40
200	200	0

The obtained standard curve (Figure 2-3) equation is A_{402} = 0.01234 * [p-NP], R^2 = 0.9999.

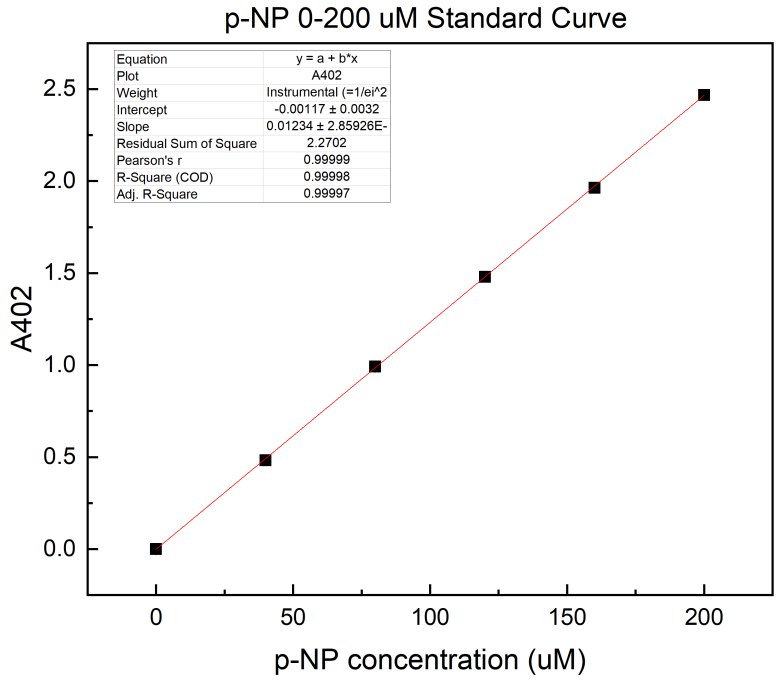

Figure 2-3. The standard relation between absorbance at 402 nm and p-NP concentration under pH 7.4 45.8 mM HEPES buffer.

Chapter 3. RESULTS AND DISCUSSION

3.1 PEPTOID SELF-ASSEMBLY PREPARATION AND CHARACTERIZATION

Inspired by the natural CA, which coordinates with three nitrogen atoms and one oxygen atom from either H_2O or OH^-, we have designed and synthesized a series peptoid with three regions: the hydrophobic region, the hydrophilic region, and a terminal coordination site. The hydrophobic region contains six N-[2-(4-bromophenyl)ethyl]glycine (NBrpe) units, which have been demonstrated essential to form nanosheets through strong π - π interactions [44]. The hydrophilic region contains N-(2-carboxyethyl) glycine (Nce) units and N-(2-aminoethyl)glycine (Nae) units in different numbers or arrangements since the hydrophilic groups are considered to be able to enhance the water network near the catalytic site. Tetraazacyclododecane-1,4,7,-three acetic acid (DO3A) was chosen as the terminal coordination group because DO3A can effectively coordinate with metal ions [45]. Following this design, the peptoid can self-assemble into nanosheets, and at the same time, the CA mimetic active site can also interact with the bulk solution. By designing and synthesizing these peptoids, I aim to demonstrate the importance of the chelating group to CA mimetic activity and establish the relationship between peptoid self-assembled nanostructures and the CA mimetic activity strength.

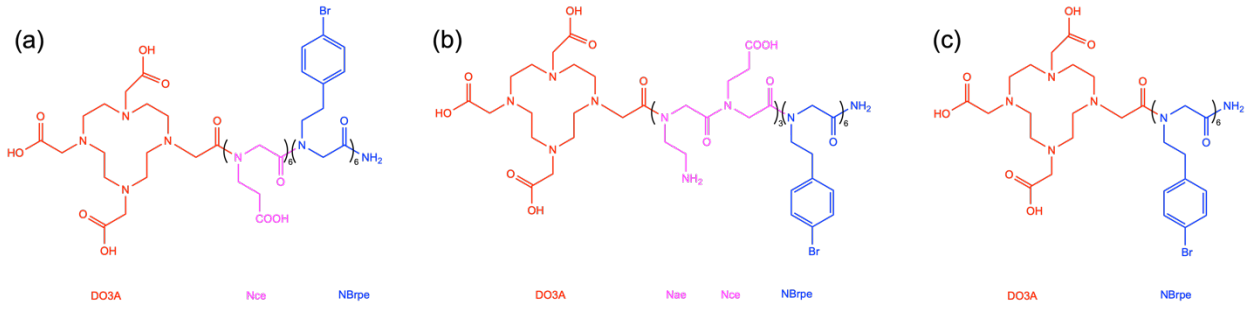

Figure 3-1. Chemical structures of CA mimic peptoids: (a) Pep-1: $NBrpe_6Nce_6DO3A$; (b) Pep-2: $NBrpe_6(NceNae)_3DO3A$; (c) Pep-3: $NBrpe_6DO3A$

Peptoid CA mimic was prepared in two steps: coordination and self-assembling. Firstly, after the peptoids have been synthesized, the active site on the peptoid needs to coordinate with a metal ion to achieve a CA mimetic activity. And during the coordination process, a pure organic solvent environment or a right aqueous solution pH is important for the Zn^{2+} to bind to the DO3A group. By combining the self-assembling process, we have exploited two methods to conduct the coordination process: (1) Treat peptoids with TFA. The 0.5 umol peptoid was dissolved in a few uL 95% TFA and dried with N_2 gas flow, followed by adding 200 uL H_2O/acetonitrile and tuning the pH to 5~6 with NaOH solution. Then the peptoid solution was lyophilized overnight to get powder containing peptoid and salts. The powder was fully dissolved in 200 uL acetonitrile, and 50 uL $Zn(BF_4)_2$ acetonitrile solution (6 eq) was added to make sure the peptoid could bind with the overdosed Zn ion. After incubating overnight, the solution was lyophilized to obtain the pep-Zn complex. (2) Treat peptoids without TFA. The powder was directly dissolved in 200 uL acetonitrile, but the peptoids did not fully dissolve at the beginning. Then, 50 uL $Zn(BF_4)_2$ acetonitrile solution (6 eq) was added. After incubating overnight, the solution became clear and was lyophilized to obtain the pep-Zn complex.

The self-assembling process was induced by evaporating the organic phase after adding a mixed solution of H_2O/acetonitrile (v/v = 1:1). For the peptoid that was previously treated with TFA and tuned pH in advance was dissolved in 200 uL H_2O/ACN and slowly evaporated under 4 ºC for two weeks. The peptoid without TFA treatment was dissolved in 200 uL H_2O/ACN, and the pH was tuned to 5~6 with NaOH, then letting the solution evaporate under 4 ºC for two weeks. The solutions became turbid in two weeks, and we filled the solution with water to 200 uL to quantify its concentration. After another week, we added another 100 uL of water to the peptoid solution to

enhance the dispersion of peptoid aggregates dispersion. The crystalline self-assembled peptoids were characterized by atomic force microscopy (AFM) and scanning transmission electron microscopy (STEM). The Pep-1-Zn (NBrpe6Nce6DO3A-Zn) (non-TFA treat) exhibited a well-defined nanosheet structure (Figure 3-2 a, d), with average sheets height of 4.3 ± 0.3 nm. However, Pep-1-Zn did not exhibit sheets-like structures through AFM and STEM characterization. Both Pep-2-Zn (NBrpe6(NceNae)3DO3A-Zn) treated with or without TFA exhibited well-defined nanosheet structures (Figure 3-2 b, c, e, f). The Pep-2-Zn has an average sheets height of 4.6 ± 0.4 for both with and without TFA treatment. However, Pep-2-Zn without TFA treatment showed more small rectangular sheet fragments than Pep-2-Zn with TFA treatment under dry-condition AFM. The Pep-1-Zn and Pep-2-Zn sheets are slightly thicker than the peptoid sheet without the chelating group reported previously [24], demonstrating that the sheet-forming peptoid increased the thickness of the sheets after conjugating a DO3A group.

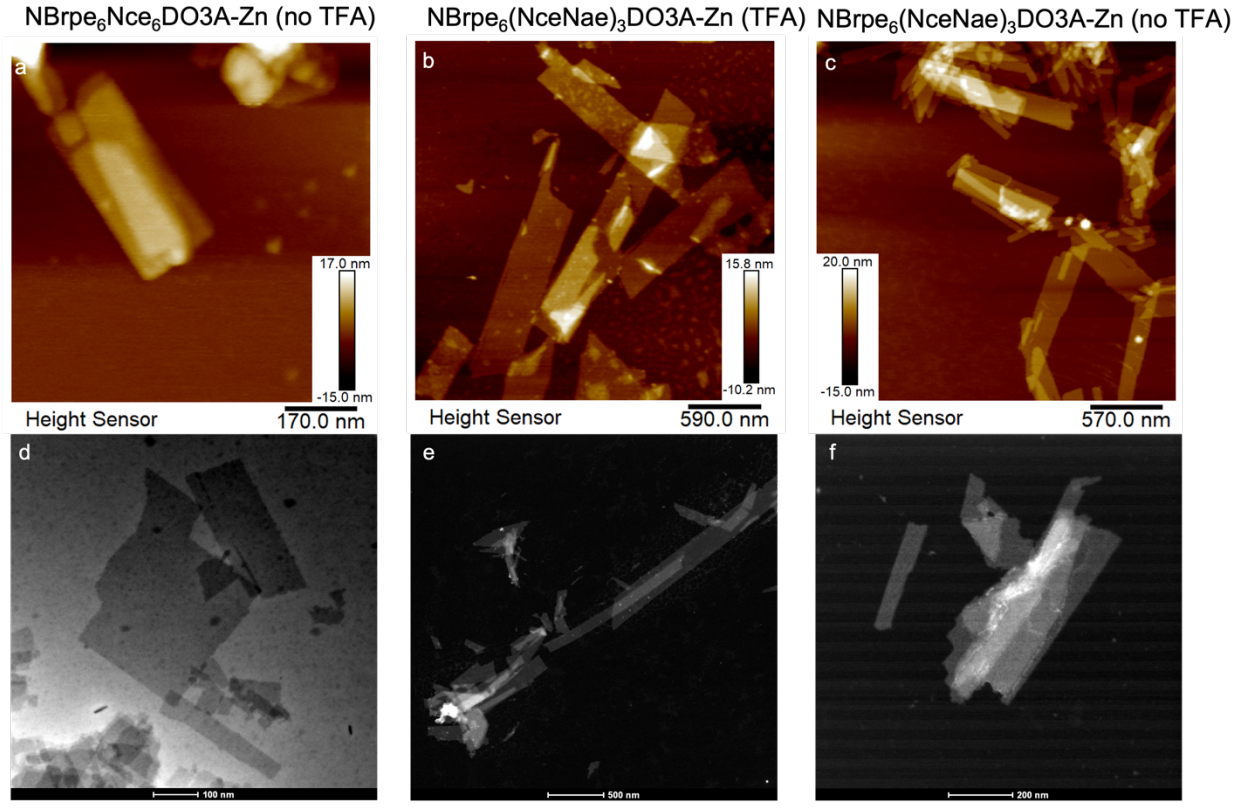

Figure 3-2. AFM and STEM images of Zn-coordinated peptoid nanostructures. (a) and (d) Pep-1-Zn without TFA treatment formed nanosheets. (b, c, e, f) Both Pep-2-Zn (NBrpe6(NceNae)3DO3A-Zn) treated with or without TFA showed self-assembled into rectangular nanosheets, while the non-TFA treated one had more sheet fragments.

3.2 CA MIMETIC ACTIVITY OF DO3A CONTAINING PEPTOID

The CA mimetic activities of Pep-1-Zn and Pep-2-Zn sheets were thoroughly assessed in their ability to catalyze the hydrolysis of p-NPA. These self-assembled peptoid sheets were incubated under 4 ºC for three weeks before the first hydrolysis experiment. After adding p-NPA to the peptoid solution with 50 mM HEPES buffer, the color of the solution gradually turned yellow, which demonstrates the degradation of p-NPA and accumulation of the colored substance p-NP in the presence of the peptoid CA mimics. The UV-vis absorbance of the solution at 402 nm (A_{402}) was measured at a certain time interval (15 min and 30 min), and the obtained A_{402} was converted into p-NP conversion according to the p-NP standard curve and the initial p-NPA concentration.

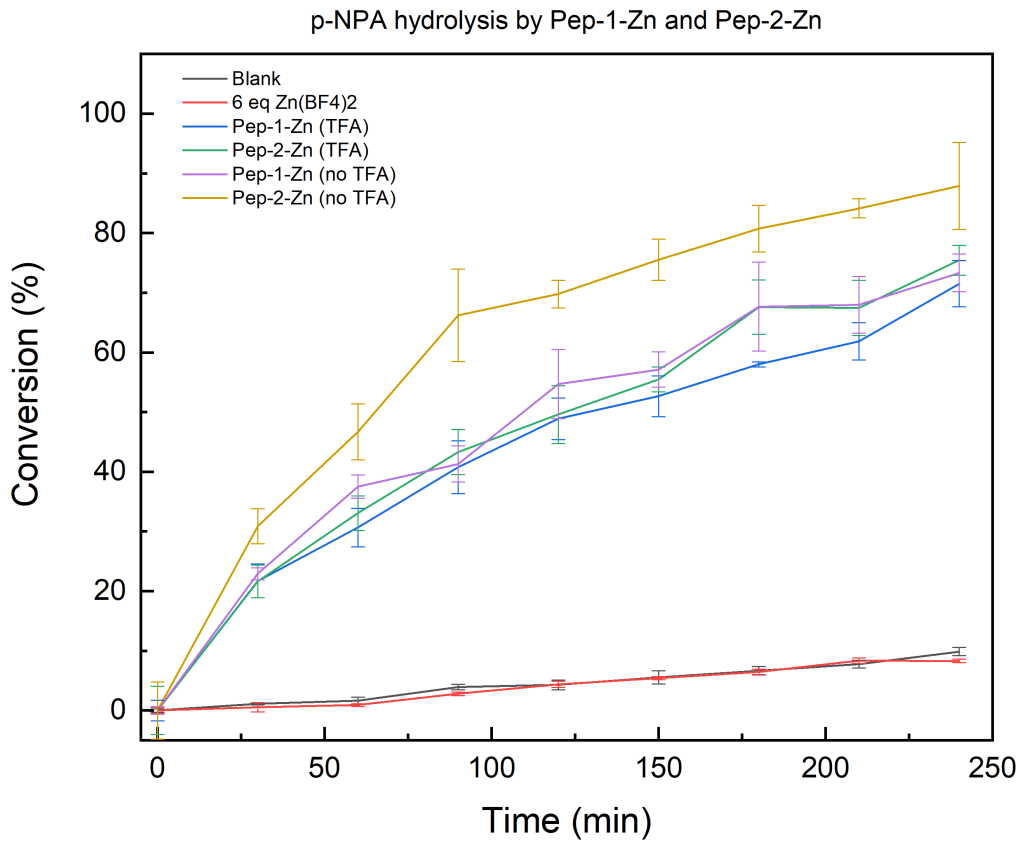

Figure 3-3. Kinetics of p-NPA hydrolysis in the presence of peptoid CA mimics, water, and Zn^{2+} ion. The reaction conditions were [Pep-1-Zn] or [Pep-2-Zn] = 13.9 uM, [p-NPA] = 166.7 uM, blank is water and HEPES buffer, Zn^{2+} group [$Zn(BF_4)_2$] = 83.3 uM.

The p-NPA hydrolysis conversion versus time curves of peptoid CA mimics and control groups are shown in Figure 3-3. In a 4 hours reaction in 50 mM pH 7.4 HEPES buffer, compared with the blank group with a very weak p-NPA conversion rate, all the peptoid CA mimics showed excellent hydrolytic activity toward p-NPA. By testing the pH of the reaction solution after 4 hours, the pH value was still at ~ 7, indicating the pH maintained during the hydrolysis reaction and excluding the hydrolysis of p-NPA was affected by the pH variation in the solution. The Pep-1-Zn (TFA), Pep-1-Zn (no TFA), and Pep-2-Zn (TFA) showed the conversion of p-NPA increased relatively fast at first, then the conversion increase was slowed slightly, as time increased similarly. Their p-

NPA conversion after 4 hours were 71.5 ± 3.9%, 75.4 ± 3.2%, 73.3 ± 2.5%, respectively. Among the four peptoid CA mimic groups, the Pep-2-Zn (no TFA) showed the highest conversion rate toward p-NPA. P-NPA was converted faster in the first 90 minutes; then the conversion increased linearly until reaching 87.9 ± 7.3% at 4 hours. The reason why the non-TFA treated Pep-2-Zn has the highest conversion rate may be that the trifluoroacetate salt in the peptoid assembling solution can reduce the DO3A binding with Zn^{2+} ion. Also, compared with Pep-1 only bearing carboxylate groups on its side chains, some amine groups on the Pep-2 side chain may increase the local pH value and provide an additional coordination site to Zn^{2+}, which can potentially increase the CA mimetic activity. Also, the reaction solution with Zn^{2+} did not show apparent hydrolytic activity compared with the blank group, which demonstrated that Zn^{2+} alone would not strengthen the H_2O deprotonation like the Zn active site on CA or CA mimics does. The coordination environment comprised of multiple nitrogens and a Zn^{2+} is crucial for the peptoid-CA mimics to achieve a hydrolytic activity.

3.3 Effect of Peptoid Concentration on CA Mimetic Activity

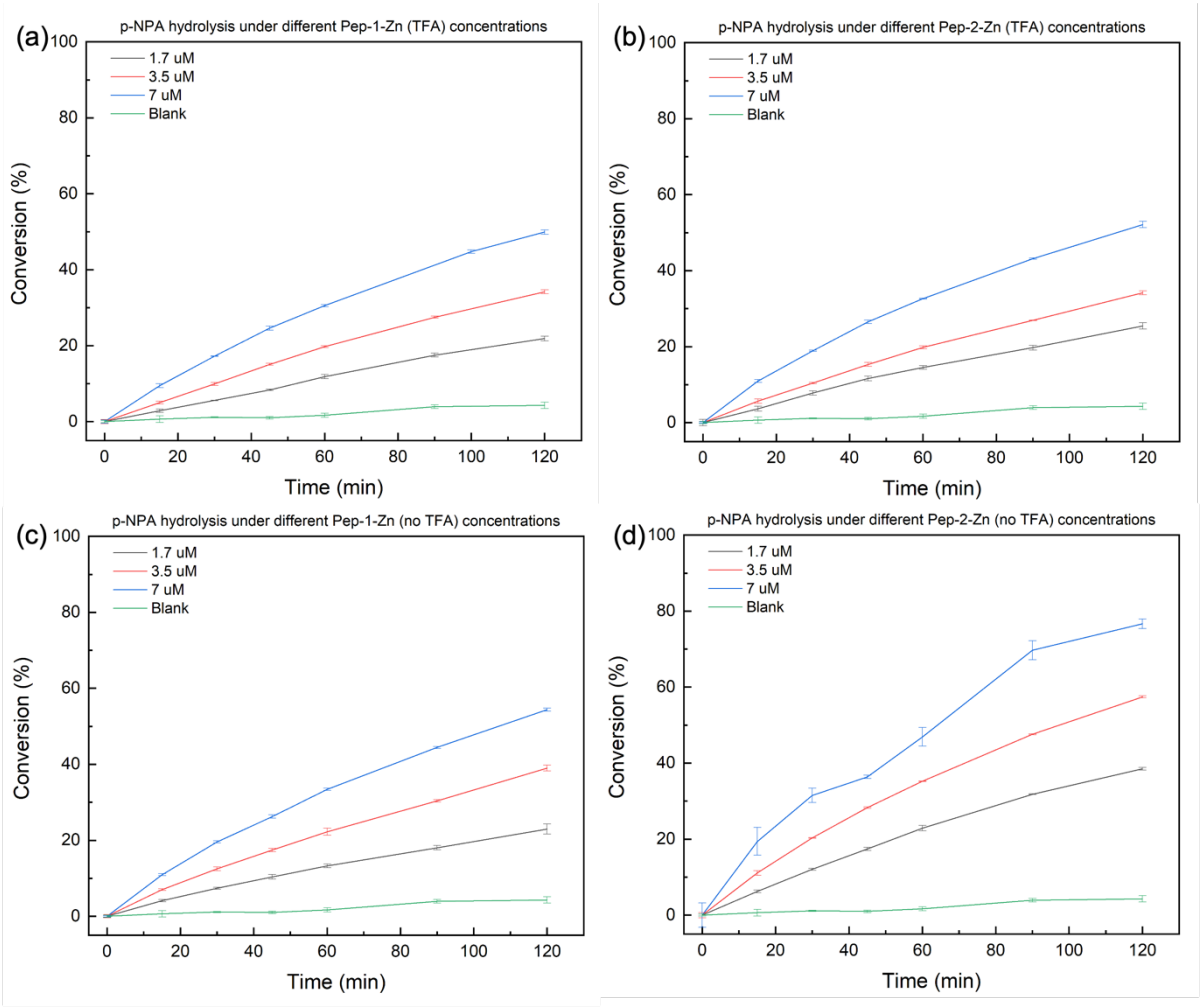

Figure 3-4. Kinetics of p-NPA hydrolysis by different concentrations of Pep-1-Zn and Pep-2-Zn

To investigate the relationship between peptoid CA mimics concentration and their activity, the kinetics of p-NPA hydrolysis was studied across different concentrations (1.7 uM, 3.5 uM, 7 uM) of Pep-1-Zn and Pep-2-Zn. As shown in Figure 3-4, all the peptoid CA mimics showed increased hydrolytic activity toward p-NPA as their concentration increased, suggesting the critical role of peptoid CA mimics in p-NPA hydrolysis. Similar to the previous result, the Pep-1-Zn (TFA), Pep-1-Zn (no TFA), and Pep-2-Zn (TFA) showed a similar trend in the conversion of p-NPA, while

the Pep-2-Zn (no TFA) showed the highest p-NPA conversion rate under each peptoid concentration (Figure 3-5). However, the p-NPA conversion did not multiply as the peptoid concentration multiplied. For example, the hydrolytic rate of 1.7 uM Pep-2-Zn (no TFA) is 0.54 uM/min, while the rate of 3.5 uM is 0.78 uM/min and the rate of 7 uM is 1.03 uM/min. The hydrolytic rate increased as the concentration increased, but the hydrolytic rate per peptoid molecule decreased, which may indicate higher efficiency under lower peptoid concentration. The effect of the peptoid concentration on the hydrolytic activity can be further investigated by saturating the peptoid concentration, which may give us insight into how the peptoid interact with the substrate.

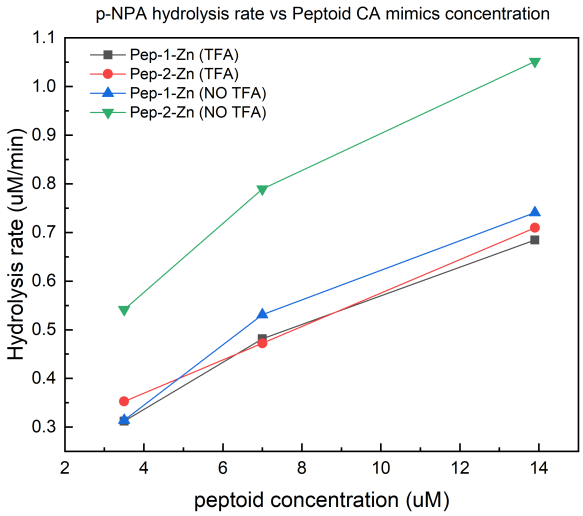

Figure 3-5. P-NPA hydrolysis rate versus peptoid concentration. The rates were gathered from the linear fitting of the first 60 minutes of the hydrolysis reaction.

3.4 Effect of Buffer and pH on CA Mimetic Activity

The p-NP accumulation is also correlated with the pH of the reaction solution. The HEPES buffer should provide a stable pH environment for p-NPA hydrolysis only affected by the factor of

difference of peptoid CA mimics rather than the solution pH. P-NPA hydrolysis in the presence of Pep-2-Zn sheets under different concentrations of pH 7.4 HEPES buffer concentrations was also conducted, shown in Figure 3-6. By varying the HEPES buffer concentrations, the conversions of p-NPA showed some differences but were still similar in trend. It demonstrated that the HEPES only would not affect the p-NPA degradation significantly.

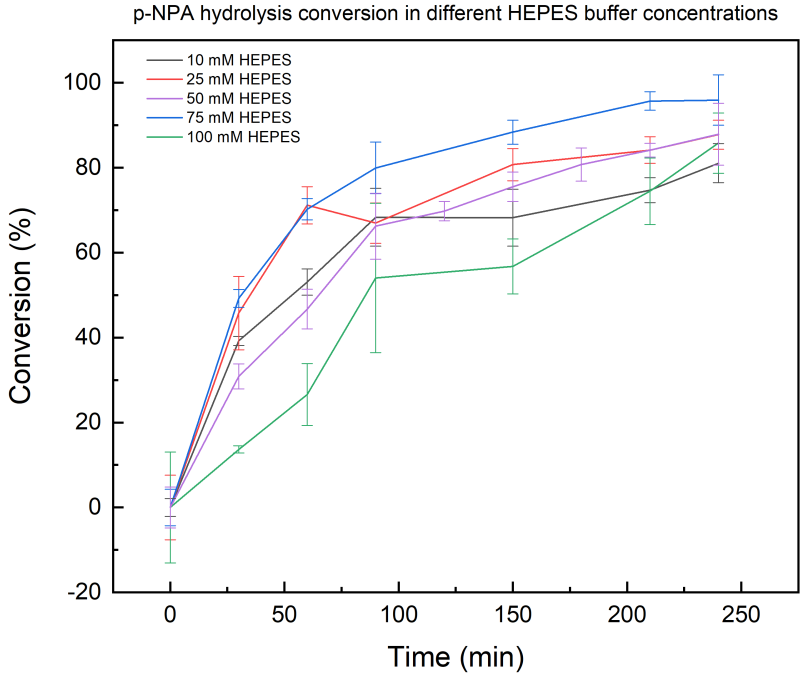

Figure 3-6. Kinetics of p-NPA hydrolysis under different HEPES buffer concentrations. In other hydrolysis experiments, 50 mM HEPES buffer was used.

The p-NPA hydrolysis kinetics curve by Pep-2-Zn (no TFA) is shown in Figure 3-7. As can be observed, the conversion of p-NPA increased linearly under each pH environment, and the conversion rate of the blank group (buffer only) was increased. In comparison, the p-NPA hydrolysis was significantly enhanced under a higher pH condition in the presence of Pep-2-Zn. The hydrolysis of p-NPA was fully converted under varying pH values at different times, with pH 8.2 in 60 minutes, and pH 9.1 just in 10 minutes to reach 100% conversion. According to the result, we speculated that the higher OH^- concentration could significantly strengthen the deprotonation

of the water molecule coordinating with the Zn more than the deprotonation of the bulk water molecule. Also, the peptoid CA mimics achieving a high catalytic efficiency under pH conditions other than physiological conditions demonstrated that the excellent stability of peptoid nanostructure is incorporated in the peptoid CA mimics. The peptoid CA mimics have the potential to be operated under an industrially alkaline environment without losing activity quickly.

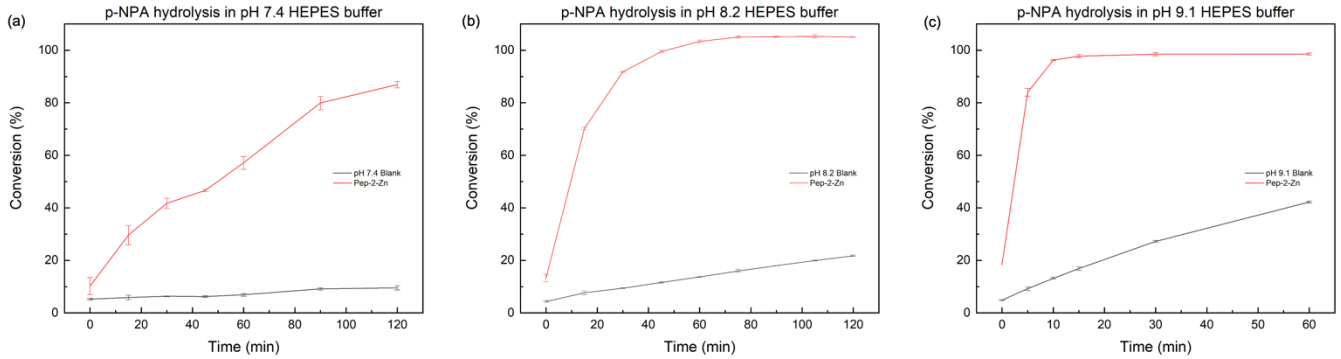

Figure 3-7. Kinetics of p-NPA hydrolysis under different pH conditions. The reaction conditions were [Pep-2-Zn] = 7 uM, [p-NPA] = 166.7 uM, and pH = 7.4, 8.2, and 9.1 for (a), (b), and (c), respectively. The conversions at 0 minutes were not set to 0 because the p-NPA degraded so fast under higher pH that the UV-vis measurement at 0 minutes could not represent the conversion at 0 minutes.

3.5 CA Mimetic Activity of Peptoid-Zn Complexes

To further explore whether the hydrolysis of CA mimetic activity is improved by the crystalline peptoid nanostructure, we prepared several peptoid-Zn complexes with the same peptoid-Zn monomer as the peptoid CA mimics but did not self-assemble into nanostructures. The peptoid-Zn complex should have a hydrolytic function toward p-NPA because of the active site comprised of Zn^{2+} and coordinating nitrogen.

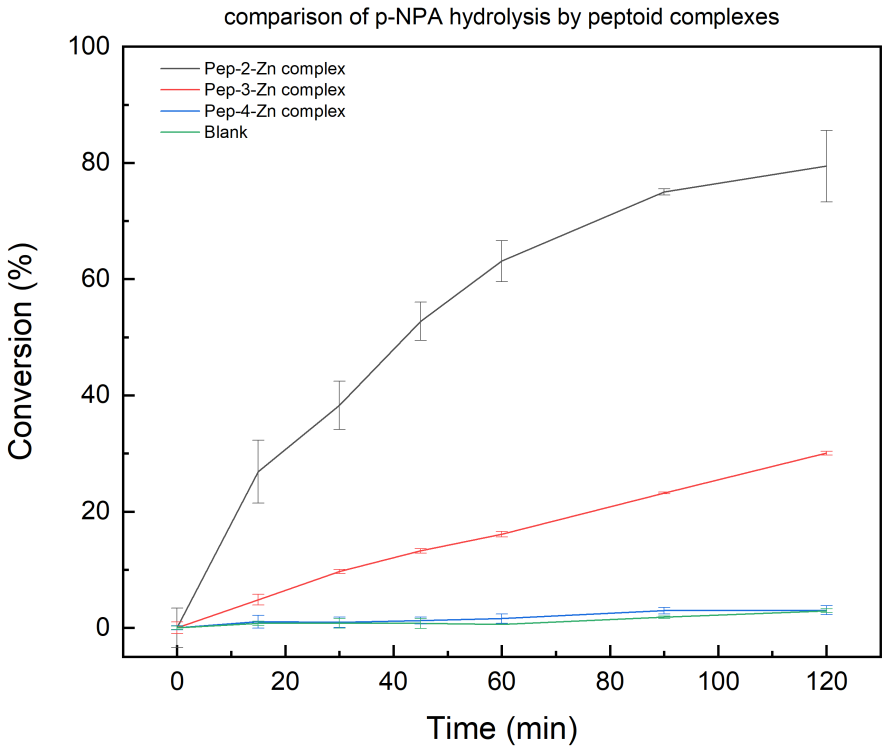

Figure 3-8. Kinetics of p-NPA hydrolysis in the presence of peptoid-Zn complexes. The reaction conditions were [Pep-2-Zn complex] = [Pep-2-Zn sheets] = [Pep-3-Zn complex] = 7 uM, and [Pep-4-Zn complex] = 83.3 uM, [p-NPA] = 166.7 uM, and pH = 7.4

Pep-2-Zn complex, Pep-3-Zn complex, and Pep-4-Zn (NBrpe6Nce6-Zn) complex were introduced to the hydrolysis reaction system. As a result, in Figure 3-8, the Pep-2-Zn complex and Pep-3-Zn complex, which process the DO3A group, were still hydrolytic active toward p-NPA. However, Pep-4-Zn, which possesses the same side chain as Pep-1-Zn but does not have a DO3A group, only showed a very weak catalytic activity similar to the blank group, which demonstrated the importance of the DO3A group to yield the hydrolytic activity. Also, the hydrolytic active Pep-2-Zn complex and Pep-3-Zn complex indicated they a sheet-like nanostructure is not necessary for the emergence of catalytic efficiency. But Pep-3-Zn, compared to Pep-2-Zn, does not have a hydrophilic domain and does not dissolve well in either aqueous condition or acetonitrile. The solubility issue of Pep-3-Zn hampers its hydrolytic activity. The Pep-2-Zn complex showed good

activity toward p-NPA with a conversion of 79.4% after 2 hours of reaction. We speculate that the enhancement of the activity of the Pep-2-Zn complex is because the longer incubation time of the peptoid in pure acetonitrile with zinc ion led to sufficient coordination between the peptoid and zinc ion. The hydrolytic efficiency of peptoid sheets CA mimics should be higher than its complex monomers due to the well-alignment of the ligands on the surface of peptoid sheets. The hydrolytic activity of complex and sheet needs to be further studied by precisely controlling the incubation time, peptoid concentration, and zinc amount.

3.6 Some Other Potential Peptoid Self-Assemblies That Could Be Used for Developing CA Mimics

Because peptoids can be easily controlled to self-assemble into various highly ordered crystalline nanostructures, we have also investigated several other self-assembling peptoid systems as potential CA mimics. In these short peptoid self-assembling systems, the hydrophobic region of these peptoids consists of four to six same hydrophobic monomers N-(2-phenylmethyl)glycine (Npm). The hydrophilic regions are a series of short molecular structures, including diglycolic acid (Dig), one glycine and alanine (Nc_2Ala), glycine (Nc_2), β-Alanine (Nc_3), and succinic acid (Suc), as shown in Figure 3-9. We have investigated their self-assembly morphologies under various conditions.

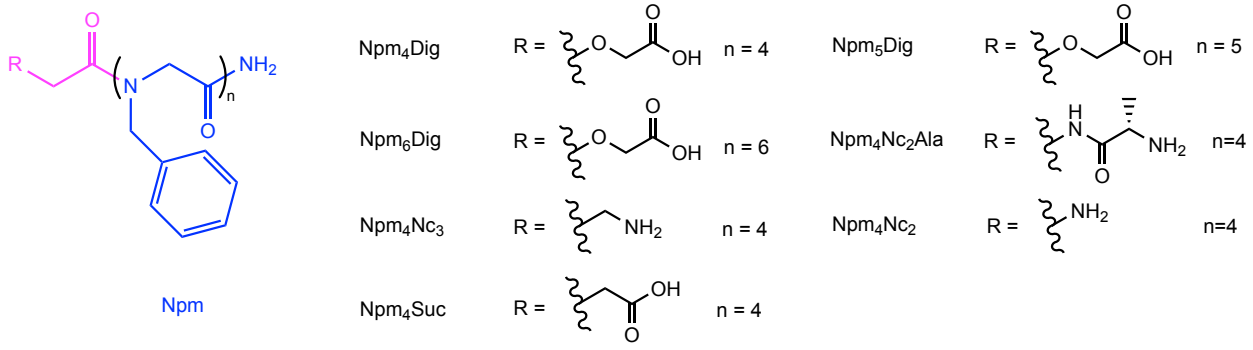

Figure 3-9. Chemical structures of Npm series peptoids

The self-assembling process of these peptoids was also triggered by adding the H2O/acetonitrile (v/v = 1:1) and evaporating the organic phase. After three days of evaporation, Npm4Dig, Npm4Nc2Ala, and Npm4Suc formed a transparent gel-like solution, while the Npm5Dig and Npm4Nc2 formed a white sticky aggregate. Npm6Dig precipitated out to form fine white sediments. And Npm4Nc3 solution was maintained clear after three days of evaporation but finally formed a gel-like solution after more than two weeks. These self-assembled peptoids were characterized by AFM, and they were all self-assembled into certain types of morphologies. The Npm4Dig, a non-chiral molecule, formed long 1-D nanohelices with a height of 6.3 ± 1 nm, shown in Figure 3-10 (a). The Npm5Dig, which has one more hydrophobic monomer Npm than the Npm4Dig, rather than forming a helical structure, could form nanorods with single rod height ranging from 13.4 nm to 39.7 nm (Figure 3-10 (b)). The Npm6Dig, which has a similar chemical composition as the previous two peptoids, can self-assemble into nanosheets with an average height of 2.6 nm ± 0.3 nm and can be a few microns in length and width (Figure 3-10 (c)). The chemical structure of Npm6Dig and the sheet height resembled the Ncpe6Nce6 sheet, which may indicate that Npm6Dig sheets have a similar packing pattern as Ncpe6Nce6. The change in the number of hydrophobic blocks can greatly influence the short peptoid self-assembly nanostructure, which demonstrates the importance of the hydrophobic domain in controlling the self-assembling pathway and the final morphologies. Furthermore, the solution pH charge effect can also affect the morphologies of Npm6Dig self-assemblies. As shown in Figure 3-11, the Npm6Dig self-assembled into helices and sheets under an acid condition, while they could only form sheets under neutral and basic conditions. We speculate that the protonation state of the Dig group may influence the self-assembly pathway.

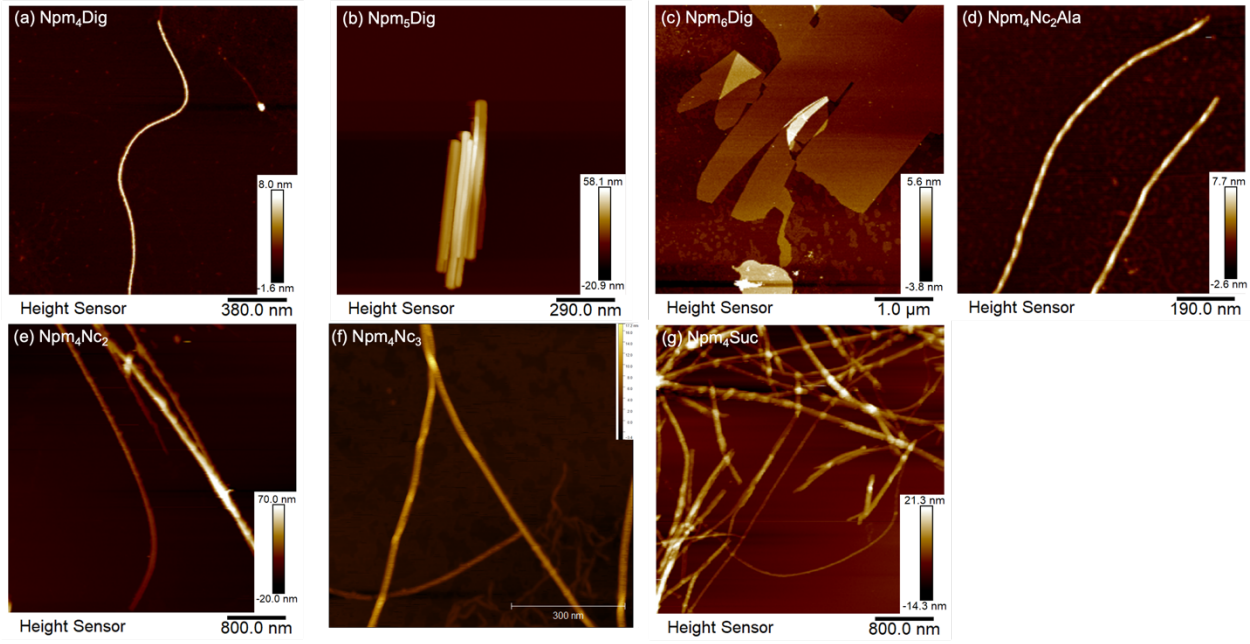

Figure 3-10. AFM images of peptoid self-assemblies. (a) Npm4Dig. (b) Npm5Dig. (c) Npm6Dig. (d) Npm4Nc2Ala. (e) Npm4Nc3. (f) Npm4Nc2. (g) Npm4Suc.

The peptoid Npm4Nc2Ala is a helix-forming peptoid whose helicity can be tuned by changing the chirality of the end group alanine (Figure 3-10 (d)). The thick height and thin height of the helices observed were 7.2 ± 0.6 nm and 5.8 nm ± 0.7 nm, respectively. The Npm4Nc2 has one amino acid glycine as an end group and can self-assemble into nanorods with heights ranging from 27 nm to 111 nm (Figure 3-10 (e)). However, the Npm4Nc3, which is only one methylene more than Npm4Nc2, can self-assemble into 1-D nanohelices with a height of thick height is 11.8 ± 1 nm and the thin height is 9.2 ± 0.3 nm (Figure 3-10 (f)). There is evidence observed that the number of methylene units can affect the helicity of peptide nanohelices [46], and this phenomenon may also occur on peptoid helices. The Npm4Suc, which has a succinic acid as its end group and is only one ether oxygen less than Npm4Dig, can also self-assemble into nanohelices (Figure 3-10 (g)).

However, these helices have a wide range of heights about 7.3 ± 2.1 nm, and longer pitch distances. All these peptoids have the ability to self-assemble into well-defined nanostructures, potentially to be further developed as CA mimics by incorporating the functioning group into these peptoids for creating active sites that mimic CAs during peptoid assembling into crystalline nanomaterials.

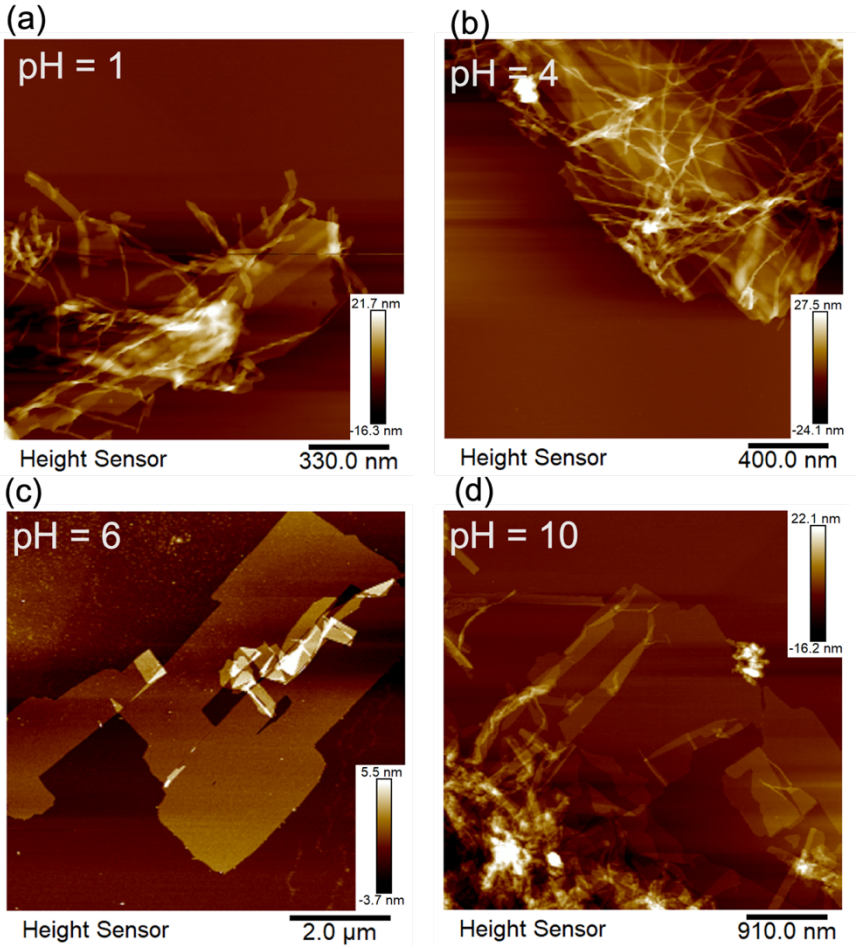

Figure 3-11. AFM images of Npm6Dig assemblies self-assembled under pH =1 (a), pH = 4 (b), pH = 6 (c), and pH = 10 (d).

Chapter 4. CONCLUSION

In this research, we have designed and synthesized several CA mimic peptoids with three regions: the hydrophobic region, the hydrophilic region, and a terminal coordination site that can bind with Zn^{2+}. These peptoids could coordinate with Zn^{2+} in a pure acetonitrile condition and self-assemble into nanosheets confirmed by AFM and TEM characterization. We demonstrated that the side-chain chemistry of peptoid building blocks, like the number of peptoid monomers and the degree of hydrophilicity, could affect the hydrolytic activity toward p-NPA. We also showed that the hydrolytic activity of the peptoid was enhanced under a basic condition. The crystalline peptoid nanostructure can also provide more unit hydrolytic efficiency than the peptoid-Zn complexes. Finally, we designed and synthesized several short peptoid sequences capable of self-assembling into various nanostructures, which could potentially serve as templates for building CA mimics in the future. Although the CA mimic peptoids are still not comparable to the natural CAs at the current stage like the turnover number per active site, we can introduce more active sites to the peptoid to compensate for the limitation. And though carefully designing the hydrophilic domain of the peptoids and choosing other Zn-binding ligands should also improve the hydrolytic activity of the peptoid. Overall, these peptoid-based CA mimics could represent significant advancements in CO_2 hydration for promoting CO_2 sequestering and storage.

BIBLIOGRAPHY

[1] J.F.B. Mitchell, The “Greenhouse” effect and climate change, Reviews of Geophysics. 27 (1989) 115–139. https://doi.org/10.1029/RG027i001p00115.

[2] H. Ritchie, M. Roser, P. Rosado, CO_2 and Greenhouse Gas Emissions, Our World in Data. (2020). https://ourworldindata.org/co2-and-greenhouse-gas-emissions (accessed March 22, 2023).

[3] R. Occhipinti, W.F. Boron, Role of Carbonic Anhydrases and Inhibitors in Acid–Base Physiology: Insights from Mathematical Modeling, International Journal of Molecular Sciences. 20 (2019) 3841. https://doi.org/10.3390/ijms20153841.

[4] A. Nocentini, C.T. Supuran, C. Capasso, An overview on the recently discovered iota-carbonic anhydrases, Journal of Enzyme Inhibition and Medicinal Chemistry. 36 (2021) 1988–1995. https://doi.org/10.1080/14756366.2021.1972995.

[5] J.K. Kim, C. Lee, S.W. Lim, A. Adhikari, J.T. Andring, R. McKenna, C.-M. Ghim, C.U. Kim, Elucidating the role of metal ions in carbonic anhydrase catalysis, Nat Commun. 11 (2020) 4557. https://doi.org/10.1038/s41467-020-18425-5.

[6] R.R. Crichton, Zinc – Lewis Acid and Gene Regulator, in: Biological Inorganic Chemistry, Elsevier, 2012: pp. 229–246. https://doi.org/10.1016/B978-0-444-53782-9.00012-7.

[7] W.C. Floyd, S.E. Baker, C.A. Valdez, J.K. Stolaroff, J.P. Bearinger, J.H. Satcher, R.D. Aines, Evaluation of a Carbonic Anhydrase Mimic for Industrial Carbon Capture, Environ. Sci. Technol. 47 (2013) 10049–10055. https://doi.org/10.1021/es401336f.

[8] S. Lindskog, Structure and mechanism of carbonic anhydrase, Pharmacology & Therapeutics. 74 (1997) 1–20. https://doi.org/10.1016/S0163-7258(96)00198-2.

[9] S. Liang, X.-L. Wu, M.-H. Zong, W.-Y. Lou, Zn-triazole coordination polymers: Bioinspired carbonic anhydrase mimics for hydration and sequestration of CO2, Chemical Engineering Journal. 398 (2020) 125530. https://doi.org/10.1016/j.cej.2020.125530.

[10] J.G.D. Rains, K. O’Donnelly, T. Oliver, R. Woscholski, N.J. Long, L.M.C. Barter, Bicarbonate Inhibition of Carbonic Anhydrase Mimics Hinders Catalytic Efficiency: Elucidating the Mechanism and Gaining Insight toward Improving Speed and Efficiency, ACS Catal. 9 (2019) 1353–1365. https://doi.org/10.1021/acscatal.8b04077.

[11] R. Ma, G.F. Schuette, L.J. Broadbelt, Insights into the Relationship of Catalytic Activity and Structure: A Comparison Study of Three Carbonic Anhydrase Mimics: RELATIONSHIP OF CATALYTIC ACTIVITY AND STRUCTURE, Int. J. Chem. Kinet. 46 (2014) 683–700. https://doi.org/10.1002/kin.20879.

[12] Z.S. Al-Garawi, B.A. McIntosh, D. Neill-Hall, A.A. Hatimy, S.M. Sweet, M.C. Bagley, L.C. Serpell, The amyloid architecture provides a scaffold for enzyme-like catalysts, Nanoscale. 9 (2017) 10773–10783. https://doi.org/10.1039/C7NR02675G.

[13] S.E. Wong, E.Y. Lau, H.J. Kulik, J.H. Satcher, C. Valdez, M. Worsely, F.C. Lightstone, R. Aines, Designing small-molecule catalysts for CO2 capture, Energy Procedia. 4 (2011) 817–823. https://doi.org/10.1016/j.egypro.2011.01.124.

[14] M.M. Ibrahim, M.A. Amin, K. Ichikawa, Synthesis and characterization of benzimidazole-based zinc complexes as structural carbonic anhydrase models and their applications towards CO2 hydration, Journal of Molecular Structure. 985 (2011) 191–201. https://doi.org/10.1016/j.molstruc.2010.10.041.

[15] A.M. Wright, Z. Wu, G. Zhang, J.L. Mancuso, R.J. Comito, R.W. Day, C.H. Hendon, J.T. Miller, M. Dincă, A Structural Mimic of Carbonic Anhydrase in a Metal-Organic Framework, Chem. 4 (2018) 2894–2901. https://doi.org/10.1016/j.chempr.2018.09.011.
[16] C. Jin, S. Zhang, Z. Zhang, Y. Chen, Mimic Carbonic Anhydrase Using Metal–Organic Frameworks for CO_2 Capture and Conversion, Inorg. Chem. 57 (2018) 2169–2174. https://doi.org/10.1021/acs.inorgchem.7b03021.
[17] N. Singh, M. Kumar, J.F. Miravet, R.V. Ulijn, B. Escuder, Peptide-Based Molecular Hydrogels as Supramolecular Protein Mimics, Chemistry – A European Journal. 23 (2017) 981–993. https://doi.org/10.1002/chem.201602624.
[18] D.J. Mikolajczak, B. Koksch, Peptide–Gold Nanoparticle Conjugates as Artificial Carbonic Anhydrase Mimics, Catalysts. 9 (2019) 903. https://doi.org/10.3390/catal9110903.
[19] M.L. Zastrow, A.F.A. Peacock, J.A. Stuckey, V.L. Pecoraro, Hydrolytic catalysis and structural stabilization in a designed metalloprotein, Nature Chem. 4 (2012) 118–123. https://doi.org/10.1038/nchem.1201.
[20] C.-L. Chen, N.L. Rosi, Peptide-Based Methods for the Preparation of Nanostructured Inorganic Materials, Angewandte Chemie International Edition. 49 (2010) 1924–1942. https://doi.org/10.1002/anie.200903572.
[21] J. Sun, X. Jiang, R. Lund, K.H. Downing, N.P. Balsara, R.N. Zuckermann, Self-assembly of crystalline nanotubes from monodisperse amphiphilic diblock copolypeptoid tiles, Proceedings of the National Academy of Sciences. 113 (2016) 3954–3959. https://doi.org/10.1073/pnas.1517169113.
[22] H. Jin, Y.-H. Ding, M. Wang, Y. Song, Z. Liao, C.J. Newcomb, X. Wu, X.-Q. Tang, Z. Li, Y. Lin, F. Yan, T. Jian, P. Mu, C.-L. Chen, Designable and dynamic single-walled stiff nanotubes assembled from sequence-defined peptoids, Nat Commun. 9 (2018) 270. https://doi.org/10.1038/s41467-017-02059-1.
[23] K.T. Nam, S.A. Shelby, P.H. Choi, A.B. Marciel, R. Chen, L. Tan, T.K. Chu, R.A. Mesch, B.-C. Lee, M.D. Connolly, C. Kisielowski, R.N. Zuckermann, Free-floating ultrathin two-dimensional crystals from sequence-specific peptoid polymers, Nature Mater. 9 (2010) 454–460. https://doi.org/10.1038/nmat2742.
[24] H. Jin, F. Jiao, M.D. Daily, Y. Chen, F. Yan, Y.-H. Ding, X. Zhang, E.J. Robertson, M.D. Baer, C.-L. Chen, Highly stable and self-repairing membrane-mimetic 2D nanomaterials assembled from lipid-like peptoids, Nat Commun. 7 (2016) 12252. https://doi.org/10.1038/ncomms12252.
[25] E.J. Robertson, A. Battigelli, C. Proulx, R.V. Mannige, T.K. Haxton, L. Yun, S. Whitelam, R.N. Zuckermann, Design, Synthesis, Assembly, and Engineering of Peptoid Nanosheets, Acc. Chem. Res. 49 (2016) 379–389. https://doi.org/10.1021/acs.accounts.5b00439.
[26] H.K. Murnen, A.M. Rosales, J.N. Jaworski, R.A. Segalman, R.N. Zuckermann, Hierarchical Self-Assembly of a Biomimetic Diblock Copolypeptoid into Homochiral Superhelices, J. Am. Chem. Soc. 132 (2010) 16112–16119. https://doi.org/10.1021/ja106340f.
[27] M. Zhao, K.J. Lachowski, S. Zhang, S. Alamdari, J. Sampath, P. Mu, C.J. Mundy, J. Pfaendtner, J.J. De Yoreo, C.-L. Chen, L.D. Pozzo, A.L. Ferguson, Hierarchical Self-Assembly Pathways of Peptoid Helices and Sheets, Biomacromolecules. 23 (2022) 992–1008. https://doi.org/10.1021/acs.biomac.1c01385.

[28] S. Sivagnanam, K. Das, I. Pan, A. Barik, A. Stewart, B. Maity, P. Das, Functionalized Fluorescent Nanostructures Generated from Self-Assembly of a Cationic Tripeptide Direct Cell-Selective Chemotherapeutic Drug Delivery, ACS Appl. Bio Mater. 6 (2023) 836–847. https://doi.org/10.1021/acsabm.2c00996.

[29] N. A. Merrill, F. Yan, H. Jin, P. Mu, C.-L. Chen, M. R. Knecht, Tunable assembly of biomimetic peptoids as templates to control nanostructure catalytic activity, Nanoscale. 10 (2018) 12445–12452. https://doi.org/10.1039/C8NR03852J.

[30] F. Yan, L. Liu, T.R. Walsh, Y. Gong, P.Z. El-Khoury, Y. Zhang, Z. Zhu, J.J. De Yoreo, M.H. Engelhard, X. Zhang, C.-L. Chen, Controlled synthesis of highly-branched plasmonic gold nanoparticles through peptoid engineering, Nat Commun. 9 (2018) 2327. https://doi.org/10.1038/s41467-018-04789-2.

[31] B. Jin, F. Yan, X. Qi, B. Cai, J. Tao, X. Fu, S. Tan, P. Zhang, J. Pfaendtner, N.Y. Naser, F. Baneyx, X. Zhang, J.J. DeYoreo, C.-L. Chen, Peptoid-Directed Formation of Five-Fold Twinned Au Nanostars through Particle Attachment and Facet Stabilization, Angewandte Chemie. 134 (2022) e202201980. https://doi.org/10.1002/ange.202201980.

[32] R.N. Zuckermann, Peptoid origins, Biopolymers. 96 (2011) 545–555. https://doi.org/10.1002/bip.21573.

[33] J. Sun, R.N. Zuckermann, Peptoid Polymers: A Highly Designable Bioinspired Material, ACS Nano. 7 (2013) 4715–4732. https://doi.org/10.1021/nn4015714.

[34] R.N. Zuckermann, T. Kodadek, Peptoids as potential therapeutics, Curr. Opin. Mol. Ther. 11 (2009) 299–307.

[35] B. Cai, Z. Li, C.-L. Chen, Programming Amphiphilic Peptoid Oligomers for Hierarchical Assembly and Inorganic Crystallization, Acc. Chem. Res. 54 (2021) 81–91. https://doi.org/10.1021/acs.accounts.0c00533.

[36] H. Tran, S.L. Gael, M.D. Connolly, R.N. Zuckermann, Solid-phase Submonomer Synthesis of Peptoid Polymers and their Self-Assembly into Highly-Ordered Nanosheets, JoVE. (2011) 3373. https://doi.org/10.3791/3373.

[37] M. Monahan, B. Cai, T. Jian, S. Zhang, G. Zhu, C.-L. Chen, J.J. De Yoreo, B.M. Cossairt, Peptoid-directed assembly of CdSe nanoparticles, Nanoscale. 13 (2021) 1273–1282. https://doi.org/10.1039/D0NR07509D.

[38] M. Monahan, M. Homer, S. Zhang, R. Zheng, C.-L. Chen, J. De Yoreo, B.M. Cossairt, Impact of Nanoparticle Size and Surface Chemistry on Peptoid Self-Assembly, ACS Nano. 16 (2022) 8095–8106. https://doi.org/10.1021/acsnano.2c01203.

[39] T. Jian, Y. Zhou, P. Wang, W. Yang, P. Mu, X. Zhang, X. Zhang, C.-L. Chen, Highly stable and tunable peptoid/hemin enzymatic mimetics with natural peroxidase-like activities, Nat Commun. 13 (2022) 3025. https://doi.org/10.1038/s41467-022-30285-9.

[40] C. Zhang, X. Xue, Q. Luo, Y. Li, K. Yang, X. Zhuang, Y. Jiang, J. Zhang, J. Liu, G. Zou, X.-J. Liang, Self-Assembled Peptide Nanofibers Designed as Biological Enzymes for Catalyzing Ester Hydrolysis, ACS Nano. 8 (2014) 11715–11723. https://doi.org/10.1021/nn5051344.

[41] M. Bélières, N. Chouini-Lalanne, C. Déjugnat, Synthesis, self-assembly, and catalytic activity of histidine-based structured lipopeptides for hydrolysis reactions in water, RSC Adv. 5 (2015) 35830–35842. https://doi.org/10.1039/C5RA02853A.

[42] G. Gulseren, M. Aref Khalily, A. B. Tekinay, M. O. Guler, Catalytic supramolecular self-assembled peptide nanostructures for ester hydrolysis, Journal of Materials Chemistry B. 4 (2016) 4605–4611. https://doi.org/10.1039/C6TB00795C.

[43] M.L. Zastrow, A.F.A. Peacock, J.A. Stuckey, V.L. Pecoraro, Hydrolytic catalysis and structural stabilization in a designed metalloprotein, Nature Chem. 4 (2012) 118–123. https://doi.org/10.1038/nchem.1201.

[44] P. Mu, Designing Amphiphilic Short Peptoid Oligomers that Assemble into Crystalline Two- Dimensional Nanomaterials, M.Mat.S.E., State University of New York at Binghamton, 2022. https://www.proquest.com/docview/2775838118/abstract/3035833963054EBEPQ/1 (accessed April 4, 2023).

[45] A. Barge, E. Cappelletti, G. Cravotto, A. Ferrigato, L. Lattuada, F. Marinoni, L. Tei, Synthesis of functionalised HP-DO3A chelating agents for conjugation to biomolecules, Organic & Biomolecular Chemistry. 7 (2009) 3810–3816. https://doi.org/10.1039/B905369G.

[46] S. Misra, P. Singh, A.K. Singh, L. Roy, S. Kuila, S. Dey, A.K. Mahapatra, J. Nanda, Tuning of the Supramolecular Helicity of Peptide-Based Gel Nanofibers, J. Phys. Chem. B. 126 (2022) 10882–10892. https://doi.org/10.1021/acs.jpcb.2c06897.